Scientific Reports

https://doi.org/10.1038/s41598-026-39735-6

Article in Press

Structural investigations of sandwich coating system containing self-healing core–shell nanofibers resistant to corrosive environment

Received: 24 September 2025

Accepted: 6 February 2026

Published online: 16 February 2026

Cite this article as: Madani S.M., Sangpour P., Vaezi M.R. *et al.* Structural investigations of sandwich coating system containing self-healing core–shell nanofibers resistant to corrosive environment. *Sci Rep* (2026). https://doi.org/10.1038/s41598-026-39735-6

S. M. Madani, P. Sangpour, M. R. Vaezi & B. Ramezanzadeh

Structural investigations of sandwich coating system containing self-healing core-shell nanofibers resistant to corrosive environment

S.M. Madani[a], P.Sangpour[a], M.R.Vaezi[a], B.Ramezanzadeh[b]

[a] Department of Nano-technology and Advanced Materials, Materials and Energy Research Center(MERC), Karaj, P.O. Box 31787-316, Iran

[b] Department of Surface Coatings and Corrosion, Institute for Color Science and Technology, P.O. Box 16765-654, Tehran, Iran

Corresponding author: Sangpour@merc.ac.ir

Abstract

The protection of metallic infrastructure against corrosion remains a significant and ongoing challenge across various industrial sectors. Conventional protective coatings often deteriorate over time, particularly when exposed to mechanical damage or harsh environments, compromising their barrier function. In response to this limitation, there is increasing interest in developing multifunctional "smart" coatings that combine long term corrosion resistance with inherent self-healing capabilities. Such systems, particularly those that incorporate nanomaterials and stimuli responsive architectures, show considerable promise for enhancing structural durability and extending service life.

In this study, we engineered a corrosion resistance and self-healing coating by fabricating an epoxy matrix reinforced with silanized graphene oxide and embedded with polydimethylsiloxane (PDMS)-polyvinyl alcohol (PVA) core-shell nanofibers. The core-shell nanofibers were produced via coaxial electrospinning, utilizing PVA shell solutions at concentrations of 7, 10, and 15 wt.%. The morphology and structural integrity of the nanofibers were characterized using field emission scanning electron microscopy (FE-SEM). Additionally, complementary analyses through transmission electron microscopy (TEM), fluorescence microscopy, and Fourier-transform infrared spectroscopy (FTIR) confirmed the successful coaxial configuration, with PDMS uniformly encapsulated within the PVA shell.

We systematically evaluated the corrosion resistance and autonomous healing performance of the developed coatings through electrochemical impedance spectroscopy (EIS) under two experimental conditions: immersion of intact (unscratched) coatings for up to 148 days, and immersion of deliberately scratched coatings for up to 16 days. Accelerated corrosion testing was also conducted using the salt spray (fog) method. To assess the evolution of damage and healing at the microscale, we examined the scratch regions using FE-SEM coupled with

energy dispersive X-ray spectroscopy (EDS). The self-healing functionality correlated strongly with the high areal density and homogeneous distribution of the core-shell nanofibers within the coating matrix, ensuring a consistent and adequate release of the PDMS based healing agent upon damage. Notably, FE-SEM micrographs acquired after 480 hours of exposure demonstrated complete closure and restoration of the scratched region, confirming the effectiveness of the embedded self-healing mechanism.

Keywords: Self-healing, core-shell, nanofiber, PDMS-PVA, coating, corrosion

Introduction

Epoxy coatings are among the most widely used organic materials for protecting metallic structures in corrosive environments, owing to their excellent adhesion to metal surfaces and high crosslink density. They function by forming a protective barrier that shields the underlying metal from corrosive agents. However, these coatings do not offer a complete barrier against the diffusion of corrosive ions [1–3]. During service, defects such as microcracks or physical damage can develop in the organic coating, allowing corrosive species in the surrounding solution to reach the metal surface and initiate corrosion.

Organic coatings are not perfect, defect-free barriers; aggressive species such as chloride ions, oxygen, and water can penetrate through them. When this occurs, corrosion initiates at the coating/metal interface beneath the coating. The corrosion reactions in this confined region closely resemble those occurring in bulk electrolyte solutions, with the critical distinction that corrosion is localized to a very small area beneath the coating. Consequently, due to the limited volume of electrolyte present in this microenvironment, rapid and significant fluctuations in pH and ionic concentration are commonly observed. The electrolyte accumulated beneath the coating not only promotes metal corrosion but also gradually degrades the coating itself, reducing its adhesion to the underlying metal substrate. The concurrent action of these two phenomena corrosion and coating delamination significantly compromises the overall protective performance of the coating system. Moreover, organic coatings can deteriorate due to factors beyond electrochemical corrosion. Mechanical impacts, abrasion, cracking, and micro-scratching induced by mechanical deformation, as well as photo oxidative degradation caused by ultraviolet (UV) radiation, can all inflict damage on the coating integrity. Critically, all these degradation mechanisms create preferential pathways for the ingress of ambient moisture and atmospheric species into the sub-coating region, thereby initiating corrosion at the metal/coating interface [4-7].

Most self-healing coatings are designed to recover their protective properties after minor damage. Healing typically occurs at microcrack sites, preventing crack propagation and inhibiting the penetration of water, oxygen, and corrosive ions to the substrate. In this way, the integrity of the metal substrate is preserved against corrosion. Self-healing strategies have been extensively evaluated in both pretreatment and topcoat layers, primarily through the incorporation of corrosion inhibitors either directly blended into the coating matrix or stored in embedded reservoirs [8–11].

One practical approach to implementing self-healing functionality involves the encapsulation of healing agents. Microencapsulation is a well-established method used across diverse fields including agriculture, medicine, food, textiles, adhesives, and coatings due to its compatibility with polymer composites and thin films. The amount of healing agent delivered can be precisely controlled by adjusting the microcapsule diameter. Upon mechanical damage or environmental triggers, monomers encapsulated within polymer shells are released and subsequently polymerize in the damaged region, thereby repairing the matrix. A key limitation of this approach is its single-use nature, as the healing capacity is typically not regenerable once the agent is released [12–15].

An alternative strategy employs vascular networks, in which healing agents are stored within hollow fibers or microtubes. When these conduits are ruptured due to damage, the healing agents are released and react to restore the matrix. A significant advantage of vascular systems is their potential to be connected to large, external reservoirs, enabling the repair of extensive or repeated damage. Depending on the materials and design, such networks can be engineered in one-, two-, or three-dimensional configurations [16–18].

Numerous studies have explored self-healing materials for corrosion protection. Zhang et al. [19] used hollow glass microspheres with micron sized pores as micro reservoirs for epoxy and amine healing agents to evaluate self-healing performance. They examined parameters such as fiber diameter, shell thickness, and internal cavity dimensions. Micro compression tests revealed that these microspheres exhibit relatively high compressive strength but are inherently brittle. Bekas et al. [20] incorporated multi-walled carbon nanotubes as a reinforcing nanostructure within a vascular self-healing system, embedding a low viscosity epoxy healing agent at three different weight percentages. Park et al. [17] developed a coaxial electrospinning process to fabricate core–shell spiral fibers for loading self-healing agents into an acrylate matrix. Similarly, Doan et al. [21] utilized electrospinning to produce core–shell fibers containing self-healing polymers, demonstrating the potential of electrospun

fibers as carriers for reactive agents. When mechanical damage occurs, these fibers fracture, releasing the core encapsulated healing agent to autonomously repair the affected area.

Li et al. [22] synthesized composite coatings by dispersing core–shell fibers containing healing agents into an acrylic resin matrix. The fibers were fabricated via coaxial electrospinning, with epoxy (or another healing agent) as the core and polystyrene as the shell. This modified electrospinning technique allows the core to be either liquid or solid. In self-healing applications, the liquid core serves as the healing agent, while the polymeric shell provides structural integrity and controlled release. In another vascular-inspired approach, a three-dimensional network of microtubes filled with resin and curing agent is embedded beneath the coating. When damage ruptures these tubes, the released components react to heal the defect. Importantly, if the same location is damaged again, additional healing agent remains available for subsequent repair cycles [23–25].

Core–shell self-healing materials hold significant promise for real world applications in highly corrosive or demanding environments. In marine applications, they can be integrated into protective coatings for ships, offshore platforms, and port infrastructure, offering dual functionality against both corrosion and biofouling. Their ability to autonomously heal micro cracks prevents water and chloride ion penetration, thereby extending service life and reducing maintenance costs. Similarly, in civil engineering, these materials can be applied to corrosion prone structures such as bridges, pipelines, and chemical storage tanks, where they help maintain structural integrity by healing cracks before they propagate. Beyond infrastructure, the aerospace and automotive industries can benefit from these systems in protective coatings or composite matrices, enhancing component durability under mechanical stress and environmental exposure while minimizing downtime for repairs. Despite their advantages, several limitations must be addressed before widespread adoption [26-27].

Aging due to prolonged exposure to UV radiation, moisture, and temperature fluctuations can degrade both the healing agents and the polymer matrix, diminishing self-healing efficiency over time. Notably, polyvinyl alcohol (PVA) a commonly used shell material exhibits poor environmental stability, particularly in humid or aqueous conditions, where it is susceptible to hydrolysis, leading to compromised mechanical and healing performance. Additionally, while self-healing can partially restore material properties, the healed regions often do not fully recover the original strength or toughness, especially if healing agent reservoirs are depleted or unevenly distributed. Finally, although electrospinning enables precise fabrication of core–shell nanofibers, scaling this technique for industrial production remains challenging due to

difficulties in maintaining fiber uniformity, achieving high throughput, and ensuring batch to batch consistency [28-29].

Core–shell fibers can be fabricated using a variety of techniques, each offering distinct advantages tailored to specific applications. Electrospinning is among the most widely used methods, where a polymer solution is drawn into fibers under an electric field. Core–shell architectures are achieved either by blending two immiscible polymers or more precisely through coaxial electrospinning, which employs concentric needles to independently deliver core and shell solutions. A closely related approach, coaxial electrospraying, utilizes a dual capillary system to produce core–shell particles rather than fibers, enabling efficient encapsulation of active agents within a protective shell. In another method, melt spinning offers a solvent free alternative, wherein two molten polymers are coextruded through a multiorifice spinneret and solidify into fibers with defined core and shell layers. Alternatively, phase separation during fiber formation whether via electrospinning or wet spinning can spontaneously generate core–shell morphologies when two immiscible polymers segregate during solidification, with one forming the core and the other the shell. These diverse fabrication strategies highlight the versatility of core–shell fiber design, supporting applications ranging from biomedical engineering and controlled drug delivery to advanced functional materials [30-32].

In this study, a three-layer sandwich coating system with intrinsic self-healing capability was developed to enhance corrosion resistance and extend the service life of components exposed to aggressive environments. The system consists of an epoxy silanized graphene oxide (EP-GO-Si) nanocomposite as the top and bottom layers, and a middle layer of core–shell nanofibers produced via coaxial electrospinning. This hybrid architecture integrates coaxial electrospinning with spray coating techniques and was applied to ST-12 mild steel substrates. The primary objective was to embed a self-healing mechanism within a nanocomposite coating to delay the onset of corrosion and prolong the functional lifetime of steel infrastructure.

To ensure good dispersion and strong interfacial bonding between graphene oxide and the epoxy matrix, graphene oxide was functionalized using (3-glycidyloxypropyl) trimethoxysilane (GPTMS) via a sol–gel process. Additionally, the influence of the polymer shell concentration in the core–shell nanofibers serving as the intermediate layer on corrosion protection and self-healing efficiency was systematically evaluated. Polyvinyl alcohol (PVA) shell concentrations of 7, 10, and 15 wt.% were investigated to optimize coating performance.

Novelty of this work in using core-shell nanofibers can be stated as follows: Core–shell nanofibers have been employed as nanoreservoir featuring an interconnected network to store and deliver self-healing agents within a sandwich coating system. When corrosive species, such as chloride ions from a sodium chloride environment, diffuse through the pores of the topcoat layer and reach the intermediate layer containing the core–shell fibers (which function as nanoreservoirs loaded with self-healing agents), the agents are released from the nanofiber cores. As shown in this study, the interconnected architecture of these fibers enables repeated self-healing capability in the coating system.

2. Experimental

2.1. Materials

Graphene oxide (GO) and silanized graphene were prepared by a modified Hummers and sol-gel methods respectively as published previously [33]. Epoxy resin (Epiran 01-x75, Epoxide Equivalent Weight (EEW) = 434 - 555 (g/eq)) and polyamide hardener (Crayamid115, Amine value (mg KOH/g) = 205 – 220) were purchased from Khuzestan petrochemical company. Polyvinyl alcohol (PVA, M.W=72000 $g.mol^{-1}$) used as shell was purchased from Merck company and Polydimethylsiloxane (PDMS) as healable material core of core-shell nanofiber (PDMS, M.W=6800-30000 $g.mol^{-1}$) was prepared from Sigma-Aldrich company. The carbon steel (ST-12) substrate was acquired from Foolad Mobarakeh Co. of Iran.

2.2. Preparation of three-layer sandwich nanocomposite coating system

The first layer is epoxy-graphene oxide functionalized with silane nanocomposite coating, which is used to improve adhesion to the metal substrate and prevent disbanding. The second layer is core-shell nanofibers electrospun, which is responsible for storing healable materials and providing the self-healing properties. Also, the third layer is similar to the first layer and with a greater thickness that acts as a barrier layer against the permeation of corrosive ions.

2.2.1 Steel substrate preparation

The metallic substrate was the ST-12 steel which is widely used in industry. Metallic substrate in dimensions of 2.5 cm × 6 cm × 0.1 cm were ground with silicon carbide with grit sizes of 200-600 for removing oxide rust. Subsequently, they were washed and degreased with distilled water, acetone and ethanol.

2.2.2 Preparation of epoxy-functionalized graphene oxide

In the following, the decorated GO nanosheets with silane GPTMS precursor at optimal concentration of 0.2 wt. % was added to the mixture containing toluene and subjected to a probe ultrasonic stirring in an ice bath for 10 min. Then the mixture of functionalized graphene oxide and toluene added to a certain ratio of epoxy resin (weight ratio of resin and

hardener was 1.3 to 1) and stirred for 24 hours to disperse functionalized graphene oxide. It was stirred mechanically with a blade at 1000 rpm. Next, for completely distributing the graphene in the epoxy resin, the amide hardener was added to it in the mentioned weight ratio and subjected to a mechanical stirrer and the epoxy-functionalized graphene oxide nanocomposite mixture was produced.

2.2.3 Preparation of core and shell solution

To prepare polyvinyl alcohol solutions at various concentrations, polyvinyl alcohol polymer powder was dissolved in deionized water using a magnetic stirrer. The mixture was stirred for 2 hours at 60°C until a clear solution was obtained. Additionally, to prepare the core solution, polydimethylsiloxane polymer liquid was added to ethyl acetate in sufficient quantity to create a 40% by weight solution, and this mixture was also stirred on a magnetic stirrer for 2 hours at ambient temperature.

2.2.4. Electrospinning conditions

The electrospinning parameters were: polydimethylsiloxane solution 40 wt.%, electrospinning distance 18 cm, shell feeding rate 1 $mL.h^{-1}$, core feeding rate 0.2 $mL.h^{-1}$ and in concentrations of 7, 10, and 15 wt.% polyvinyl alcohol polymer solution. The samples were named as EPGSi-7%, EPGSi-10% and EPGSi-15% respectively.

To designate the samples coated with core–shell fibers containing polyvinyl alcohol (PVA) in the shell at concentrations of 10 wt%, 7 wt%, and 15 wt% within the epoxy–graphene oxide nanocomposite coating system, the labels EPGSi-10%, EPGSi-7%, and EPGSi-15% are used. In these designations, "EP" denotes epoxy resin, "G" represents graphene oxide, "Si" refers to silane, and the appended number indicates the weight percentage of polyvinyl alcohol in the fiber shell.

Then the samples were kept at room temperature for 24 hours and finally annealed at 60°C for 24 hours.

2.2.5 Application of composite coating

The epoxy-functionalized graphene oxide was initially applied to the steel substrate using a spray technique to create the first layer of the coating system. After 30 minutes, while the surface remained slightly wet, the coated sample was placed in an electrospinning system as a collector. The coaxial electrospinning process was then carried out to produce polydimethylsiloxane-polyvinyl alcohol fibers at a voltage of 13 kV.

To form the final layer, or top coat, the epoxy-silanized graphene oxide nanocomposite mixture was sprayed onto the core-shell fibers. The samples were allowed to cure at ambient

temperature for 24 hours before being baked at 60°C for an additional 24 hours. Upon drying, the total thickness of the coating system was approximately 120 ± 10 µm.

2.3. Characterization

The structural characterization of GO and GO-SiO_2 nanosheets and epoxy-GO and epoxy-GO-SiO_2 nanocomposite coatings were reported in our previous work [24]. In present study surface chemistry of core-shell nanofiber was evaluated by FTIR BRUKER VECTOR-33 with a resolution of 4 cm^{-1} and in the wavelength range of 500 to 5000 cm^{-1}. The structure of the resulting core-shell nanofibers was revealed using TEM microscope (Zeiss-EM10C company-100 KV). FE-SEM was used to investigate the morphology of nanofibers, epoxy-silanized graphene oxide nanocomposite coating and cross-section structure of the three-layer sandwich structure epoxy-silanized graphene oxide coating containing core-shell PDMS-PVA nanofibers. Furthermore, the surface morphology of the scratch area was investigated by FE-SEM; model TESCAN MIRA3, which has a High Brightness Schottky Emitter electron gun.

Energy dispersive x-ray spectroscopy (EDS/EDX) was carried out to evaluate the elemental analysis of the scratched area and the cross-section of the three-layer epoxy-silanized graphene oxide coating containing polydimethylsiloxane-polyvinyl alcohol nanofibers. The electrochemical behaviors and the self-healing properties of the three layer nanocomposite coatings containing core-shell nanofibers were investigated by EIS method via EG&G potentiostat/galvanostat apparatus model PARSTAT 2273 and a frequency response analyzer (Princeton Applied Research Model 1025) in the frequency range (100 kHz to 10 mHz) and 50 steps per decade. Oscillation amplitude of 10 mV was used in the three-electrode cell to obtain Nyquist curves, bode and bode-phase in 3.5 wt. % sodium chloride solution. The reference electrode was Ag/AgCl saturated by KCl, the auxiliary electrode was a platinum foil and the coated metal substrate was considered as the working electrode with a surface area of 1 cm^2. To confirm the reproducibility of the data, each measurement was performed for three samples prepared under the same conditions and representative values were reported. The results were obtained using 'Zview' software. In order to investigate the protective and self-healing effect of the coating system, a deep cut was made on the coating with a sharp surgical blade, 2 cm long and 100 µm wide, to the extent that it was deep to the top of the metallic substrate. Then, the effect of immersion times on the corrosion resistance of coating systems has been performed by EIS analysis.

Salt spray test was used to evaluate the corrosion resistance and the self-healing performance of the nanocomposite coating that is widely used in the industrial substrates. Salt spray test in

accordance with ASTM B 117 standard on coating samples that are scratched (4 cm long and 2 mm wide) by a sharp surgical razor. A solution containing 5 wt. % Sodium chloride was compressed air in the chamber. The samples were kept at an angle of 15–30 degrees to the vertical. The temperature and pressure of salt spray were kept at 35±2 ^{o}C and 0.83–1.24 bar.

3. Result and discussion

3.1. Characterization of PVA-PDMS core-shell nanofibers

The FTIR spectrums related to polyvinyl alcohol fibers, polydimethylsiloxane solution and core-shell fibers (PDMS-PVA) were illustrated in Fig. 1. It is apparent from the FTIR spectrum of polyvinyl alcohol (PVA), the absorption band in the region of 3448 cm^{-1} is related to OH groups that are free or bound to the molecule. The absorption band at 2954 cm^{-1} corresponds to the symmetric stretching vibration of the alkyl group (-CH2) in polyvinyl alcohol. The absorption band at 1635 cm^{-1} region corresponds to the stretching carbonyl group (C=O), the absorption band at 1422 cm^{-1} region corresponds to CH2 groups (C–H bending vibrations), at 1100 cm^{-1} corresponds to C– O of acetyl group and at 1750 cm-1 corresponds to the stretching group C-C, all of these chemical species represent polyvinyl alcohol [34]. Si-CH3 stretching bond at 1262 cm^{-1}, Si-O-Si stretching bond at 1090-1022 cm^{-1}, Si-CH3 bending bond at 800 cm^{-1}, and C-H bond is observed at 2963 cm^{-1}, which represents the peaks observed in (PDMS) solution. Because of torsional movement along the main body, the PDMS has a low glass transition temperature of about -123 °C. Based on this characteristic in high molar volume, intermolecular force and cohesive energy density are very low. In addition, the surface tension, surface energy, solubility, and low dielectric constant of PDMS are related to the weak intermolecular force between PDMS chains. Lipophilic and hydrophobic behavior is attributed to the presence of methyl groups around the Si-O-Si polymer. The dissociation energy of the Si-O bond is equal to 1110 $kcal.mol^{-1}$, which is larger than the energy of C-O (5.85 $kcal.mol^{-1}$), C-C (6.182 kcal.mol-1) and Si-C (76 $kcal.mol^{-1}$). It is the reason for the high thermal stability of polyorganosiloxanes. The sensitivity of polysiloxanes to dehydration in acidic and basic conditions is the most important defect of these polymers, which is generated by the polarity of the Si-O bond [35]. It has also been observed from the FTIR spectrum of core-shell fibers PDMS-PVA that the presented bonds in the spectra related to PDMS and PVA are present in core-shell spectrum and no new bond that indicates the reaction of these two polymers in core-shell fibers has been observed, therefore, PDMS is well loaded to the core of nanofibers.

TEM image was used to ensure the formation of core-shell structure in PDMS-PVA nanofibers. As it illustrated in Fig. 2, the structure of the core-shell fibers has been created

with separate boundaries without nodes or defects. The continuous presence of core material within the core-shell fibers is also evident. The diameter size of the core and core-shell fiber was calculated by Image J software. As can be seen in the FE-SEM images of core-shell fibers in Fig. 3, with increasing the concentration of polymer PVA from 7 to 15 wt. % which is used as the shell, the diameter of the core-shell fibers also increased. The distribution of fibers in the case where the concentration of the shell PVA solution is 15 wt. % (Fig. 3C) is more uniform and more precipitation than the concentration of the PVA solution is 7 (Fig. 3A) and 10 wt. % (Fig. 3B). An increase in concentration causes an increase in polymer chain conflicts, which is necessary to achieve the continuity of the accelerated flow of the solution during electrospinning. Usually, with the increase in the concentration, the diameter of the fiber also increases. This is probably due to the greater resistance of the solution to pull by the loads mounted on the accelerated flow of the solution. Another reason that can be mentioned for increasing the diameter of the fibers with the increasing in the concentration of the polymer solution is that the area of the deposition of the fibers on the collecting plate is smaller at higher concentration. The increase in concentration means that the viscosity of the solution is strong enough to prevent the bending instability of the accelerated flow of the solution relative to the exit point of the needle, and in fact, this causes the fibers to accumulate in the smaller area. Therefore, the path of the accelerated flow of the solution is shortened and the tendency of the solution to fog around is reduced. In addition, this reduction of the jet path means that the solution is subjected to less tension, which increases the diameter of the fibers. Also, at higher concentrations, the amount of solvent in the solution jet is less and the solvent evaporates faster. Therefore, with the evaporation of the solvent, it becomes more difficult to pull the jet, and fibers with a larger diameter are formed on the collector [36-37]. The images related to the core-shell fibers obtained by using a fluorescent microscope, in different concentrations of the shell, as can be seen in Fig. 3, the core material is continuously placed inside the core-shell fibers, and with increase the concentration of the shell polymer solution from 7 (Fig. 3-A4) to 15 wt. % (Fig. 3-C4), the core material is loaded with a larger amount, without any defect in the path of the core material in the shell.

3.2. Characterization of sandwich nanocomposite coating system

As can be seen in Fig. 4B, the 0.2 wt. % epoxy composite coating of epoxy-functionalized graphene oxide with silane, the spreading and delamination of the graphene oxide sheets in the matrix of the epoxy coating are significantly improved after being functionalized with silane compared to the distribution of non-functionalized graphene oxide sheets (Fig. 4A).

Graphene oxide nanosheets are distributed in the epoxy polymer matrix homogeneously and uniformly. The absorption of silicon oxide nanoparticles and the binding of silane molecules on the graphene oxide nanosheets increase their distance and, as a result, decrease the hydrophilicity and increase the affinity of the particles to the polymer, which prevent the accumulation of graphene oxide sheets and cause the better distribution of graphene oxide particles. It can also be seen that the silanized graphene oxide sheets are placed inside the polymer matrix and do not protrude from the polymer matrix, which is due to the strong bond between the silane graphene oxide particles and the polymer through the terminal functional groups in the silane structure [38-39]. Fig. 4C shows the spectra of EDAX analysis taken from the epoxy-silanized graphene oxide composite coating surface, and the presence of silicon and oxygen peaks indicates the presence of silicon oxide on the coating surface.

In the EDAX analysis presented in Figure 4, the primary objective is to qualitatively demonstrate the presence of silicon on the surfaces of silane-functionalized graphene oxide sheets (as shown in the FE-SEM image in Figure 4-B). In comparison with the non-functionalized graphene oxide (Figure 4-A), the silane-functionalized graphene oxide sheets exhibit reduced agglomeration due to the presence of the silane groups. This distinction has been effectively elucidated by leveraging the imaging capabilities of scanning electron microscopy (SEM).

In silanized graphene oxide with the GPTMS precursor, the C-O-C epoxy functional group acts as an active site for reaction with the polymer matrix during resin curing. The functional groups of epoxy on silanized graphene oxide sheets are similar to epoxy groups in epoxy resin. In addition, silane molecules reduce the hydrophilicity of the graphene oxide surface and increase its compatibility with the polymer matrix [40-41]. FE-SEM cross-section image of the three-layer epoxy-silanized graphene oxide coating containing PDMS-PVA fibers in the middle layer is manifested in Fig. 5A. The thickness of each layers and their order are clearly observed in this figure, and the total thickness is about 120 μm. As clearly shown in Figure 5-A, the thickness of each layer is indicated by a specific number. The thickness of the first layer is 38 microns, the thickness of the middle layer is 16 microns, and the thickness of the top coat is 70 microns.

The cross-section of the middle layer and the presence of core-shell fibers in the middle layer are illustrated in Fig. 5B. Also, the Linear EDAX elemental analysis taken along the thickness of the epoxy-silanized graphene oxide coating system containing core-shell (PDMS-PVA) fibers is illustrated in Fig. 5C. As can be seen, the elements of carbon, oxygen, and silicon are evident in the coating system. The intensity of the silicon element has

increased in the middle layer, which indicates the presence of the PDMS core in these fibers, and it has the same intensity in the first and last two layers. Fig. 5D shows the FE-SEM image of the surface of the core-shell fibers used as the middle layer. The presence of core-shell PDMS-PVA fibers in the nanocomposite coating system is clearly identified.

3.3. Corrosion resistance and Self-healing performance of sandwich nanocomposite coating system

Fig. 6 shows the EIS curves of the EPGSi-7% sample which contains electrospun core-shell fibers with a PVA shell concentration equal to 7 wt. % at different immersion times in 3.5 wt. % sodium chloride medium. As can be seen from the EIS graphs at the initial immersion times, the diameter of the semicircle capacitive loop decreased by increasing the immersion time. The breakdown frequency was moved to the higher values, the phase angle decreased and the linear range related to the capacitance behavior in bode curves decreased. All the facts indicate a decrease in the resistance of the coating against the corrosive environment, which corresponds to decreasing the impedance value at a low frequency over time. In this case, where the PVA polymer solution with a concentration of 7 wt. % is used as the shell of the core-shell fibers, the diameter of the core-shell fibers is the lowest compared to the cases where concentrations of 10 and 15 wt. % are used. It is obvious that less healable material is loaded as the core in these fibers, which is consistent with the results of examining the morphology of these fibers. The equivalent electrical circuits (EECs) in the initial times and more immersion times are shown in Figs. 7A and 7B respectively. The presented EECs contain the elements of R_s, R_c, R_{ct}, CPE_c, CPE_{dl} and n. The extracted data in Table 1 illustrate that the second time constant appeared after 63 days, which indicates the beginning of corrosion reactions at the interface between the metal substrate and the coating system. In this coating system, the parameters of the coating resistance and the coating surface roughness present an upward trend at 46, 78, and 132 days. Since the presence of core-shell fibers and the creation of a passive barrier layer due to the release of the PDMS core self-healing function caused at 46, 78, and 132 days due to the creation of a weak and loose layer of corrosion products, the protection function of the system is covered.

Fig. 8 shows the EIS curves of the EPGSi-10% sample at different immersion times up to 148 days. The diameter of the semicircular capacitive loop in the Nyquist curve is smaller with increasing immersion time. In the bode curves of this sample, the reduction of the capacitive behavior of the coating system can be seen which shows decreasing of linear behavior. In the bode-phase curves, the phase angles decreased over a long period times and the breakdown frequency shifted to higher values. In fact, the coating system has a lower protection function

with more penetration of the corrosive solution and the destruction of the coating system. The decreasing trend of the impedance at the frequency of 10 mHz is in good agreement with the observations obtained from the impedance spectrum curves. In this case, a PVA polymer shell solution with a concentration of 10 wt. % was used for electrospinning core-shell fibers compared to the 7 wt. % cases; it has a lower reduction rate in impedance values. With the increase in the concentration of the polymer solution, due to more resistance of the solution to being stretched by the electric charges, the diameter of the shell fibers increases, and the possibility of loading more healable material, PDMS, has been provided. In this case, at times 46, 78, and 132 days, the trend of increasing the impedance of the coating system has been observed at low frequency, which is in good agreement with the behavior of the impedance spectra curves in this case. The self-healing process at 46 and 78 days has led to an increase in the protective performance of the coating system and prevented the continuation of the decreasing process. The creation of corrosion products at the interface between the metal substrate and the coating system is the reason for the relative and partial improvement of the impedance value in 132 days. The values related to fitting the impedance curves in Table 2 are in good agreement with the behavior of the impedance spectra curves. With the increase of immersion time, the resistances of the coating and the roughness parameter have decreased and the capacitor capacitance of the coating system has increased. The increasing trend of R_c and n occurred at 46, 78, and 132 days and the decreasing trend of the CPE_c occurred at this time. The occurrence of this phenomenon at 46 and 78 days is due to the self-healing function of the core-shell fibers and at the 132 days is due to the function caused by the formation of corrosion products.

According to Fig. 9, EIS curves of EPGSi-15% sample shows that the impedance at 10 mHz frequency with increasing concentration of PVA solution of shell after one day of immersion is 8.50×10^{10} $\Omega.cm^2$ which has increased compared to the concentrations of 7 and 10 wt. %. The bode curve of the EPGSi-15% after one day of immersion shows a completely linear region, which indicates the high resistance of the coating system in the initial times of immersion. According to the bode and bode-phase curves, only one time constant is observed in this specimen up to 99 days of immersion and the breakdown frequency has appeared in the low frequency range, which indicates the high protective performance of the coating system against the corrosive environment. With the increasing of the immersion time up to 29 days, the impedance value at the frequency of 10 mHz shows a downward trend, although in this case, a very small decrease rate has been seen compared to the specimen with a concentration of 7 wt. %, and the impedance value is in the order of 10^{10} $\Omega.cm^2$. In the

Nyquist curves, the immersion of the capacitive loop of the Nyquist semicircle is not complete until 99 days, which also indicates the low rate of corrosion in this coating system. By increasing the immersion time from 29 to 46 days, the impedance value has increased from 8.1×10^{9} $\Omega.cm^2$ to 1.17×10^{11} $\Omega.cm^2$ which is due to the self-healing performance of the core-shell fibers in the coating system due to the early times of immersion. In this case, with regards to the electrospinning core-shell fibers with PVA solution with a concentration of 15 wt. % and considering the morphology of these fibers, the amount of healable material is loaded in the interconnected three-dimensional network of the core-shell fibers, which provides the possibility of more healing. The extracted electrochemical parameters by fitting the impedance curves of the EPGSi-15% coating are presented in Table 3. The resistance of the coating system after one day of immersion is equal to 8.5×10^{10} $\Omega.cm^2$ and the capacitance of the coating system at this time is 1.08×10^{-10} $Sn.\Omega^{-1}.cm^{-2}$, which shows the high protection performance of the coating system in the early times of immersion. By increasing the immersion time to 46 days, the resistance of the coating system increased by more than one order, and the capacitance of the coating system also decreased by about one order, which indicates the increase in the corrosion resistance of the coating. In fact, as a result of the contact the corrosive aqueous solution with the core-shell fibers and the release of the PDMS polymer due to the dissolution of the PVA polymer shell, a passive protective layer has been created that prevents further penetration of corrosive ions into the coating system. After the penetration of the aqueous solution into the coating, the Si-OR groups are hydrolyzed and form Si-OH bonds, and then the condensation reaction occurs, and other Si-O-Si and Si-O-C bonds are formed inside the coating. With the formation of these silane bonds in the epoxy polymer matrix, the density of the cross-link increases and the penetration paths of the electrolyte in the coating system are reduced [42-44]. By increasing the immersion time to 63 days, the resistance of the coating system decreases and the capacitance of it increase to a small amount. It has been observed that by increasing the immersion time to 78 days, the resistance of the coating system increases and the capacitance of it decreases due to the self-healing function of the core-shell fibers loaded in the coating system. It should be noted that after 78 days of immersion in the corrosive solution, the resistance of the coating system is in the range of 10^{10} $\Omega.cm^2$ and it shows the preservation of the resistance of the coating system against the penetration of corrosive ions inside the coating due to the self-repairing function of the core-shell fibers.

Based on the EIS plots and the extracted data from their fitting curves in Fig. 10, it was seen that the EPGSi-15% coating system has high strength and the lowest capacitor capacity,

which has a good protective performance against the penetration of corrosive ions due to the presence of a continuous network with a high amount of self-healing siloxane material due to fibers with a higher diameter than the EPGSi-7% during 148 days of immersion. In this case, where PVA solution with a concentration of 7 wt. % is used as the shell of core-shell fibers, the diameter of the core-shell fibers is the lowest compared to the cases where concentrations of 10 and 15 wt. % are used. It is obvious that less self-healing material is loaded as the core in these fibers, which is consistent with the results of examining the morphology of these fibers. Therefore, the self-healing process in this coating system is lower than the core-shell fibers that used concentrations of 10 and 15 wt. %. The increasing trend of the resistance of the coating system and the decreasing trend of the capacitor capacity of it against the corrosive environment occurred in three times of 46, 78 and 132 days. In 46 and 78 days samples due to the self-healing performance of core-shell fibers and in 132 days sample due to the creation of a barrier layer due to the formation of corrosion products, an increase in the impedance of the coating system occurs.

3.3.2. Investigating the self-healing effect of sandwich nanocomposite coating system

EIS curves of the EPGSi-7% sample are manifested in Fig. 11. As shown in the graphs, after creating a scratch and after 24 hours of immersion, the Nyquist curves consist of two loops. The first loop at the low frequencies is related to performing electrochemical reactions at the interface between the metal substrate and the coating system, and the second loop at higher frequencies, is related to the formation of a passive barrier layer due to the release of the self-healing material from the core-shell fibers [45]. In bode and bode-phase curves, two time constants appeared in the initial 24 hours of immersion. The impedance values at low frequencies during this time have also shown a two-fold drop compared to the samples without scratches. In fact, after creating a scratch, the self-healing process occurred in the first 24 hours of immersion, but with increasing immersion time, the impedance values at low frequencies have reduced significantly. In fact, for the EPGSi-7% sample, due to using a PVA polymer solution with a low concentration of 7 wt. %, the diameter of the core-shell fibers has decreased, and the amount of loaded material is less than that of the self-healing material, resulting in a weaker self-healing process compared to 10 and 15 wt. % (which confirmed morphological investigations). The fitting results of EIS curves also show the increase of electrochemical corrosion reactions at the metal-coating interface with the decrease of R_c and R_{ct} and the increase of CPE_c and CPE_{dl} (Table 4).

The EIS curves of the EPGSi-10% sample are illustrated in Fig. 12. As can be seen, the semicircle diameter of Nyquist curves has increased in 36 hours compared to the initial 24

hours, and the impedance values have increased at low frequency, which indicates the self-healing process at 36 hours of immersion. In this scenario, an artificial scratch was introduced into the coating, and the coated sample was subsequently immersed in a sodium chloride solution. Electrochemical impedance spectroscopy (EIS) measurements were performed after the initial 24-hour immersion period. Due to the presence of the scratch, which facilitates easier diffusion of corrosive ions into the coating system, the scratched sample exhibited a more rapid decline in impedance compared to unscratched specimens. As immersion continued, corrosive species from the aqueous electrolyte reached the intermediate layer containing the core–shell fibers. The shell of these fibers—composed of the hydrophilic polymer polyvinyl alcohol (PVA)—dissolved upon contact with water, triggering the release of the encapsulated silane-based self-healing agent [46-47].

Subsequently, as described in the mechanism section, this agent underwent hydrolysis and condensation reactions, leading to the formation of a hydrophobic, passive barrier layer at the damaged site. This in situ generated protective layer effectively inhibited further ion ingress and corrosion diffusion, thereby increasing the coating's impedance and enhancing its corrosion resistance through self-healing [48-49].

Subsequently, with the increase of immersion time, the impedance values have decreased, and the capacitance range and phase angles have decreased [50]. At time 12 days, two capacitive loops can be seen in the Nyquist curves, one at low frequencies, which is related to the corrosion reactions at the interface between the metal substrate and the coating system, and another at the higher frequencies, which is related to the destruction of the coating system. Based on the reported information in Table 5, R_c, R_{ct} and parameter n increased at 36 hours of immersion compared to 24 hours of immersion, also CPE_c and CPE_{ct} decreased, which indicates the formation of a passive barrier film in the path of diffusion of the corrosive solution and prevention of corrosion reactions.

Damage-induced diffusion denotes the migration of atoms or ions through a material facilitated by structural damage—such as cracks, voids, or defects—which compromises the material's integrity and can accelerate degradation processes like corrosion by enabling greater ingress of environmental agents such as moisture or aggressive chemicals; this diffusion is typically governed by concentration gradients, thermal energy, and localized stress fields. In contrast, self-healing represents an autonomous repair mechanism wherein materials recover from damage without external intervention, either through the release of encapsulated healing agents or intrinsic molecular reorganization that seals microcracks, thereby restoring mechanical and functional properties and extending service life. In the

context of electrochemical characterization, the inference of passive film formation—often deduced from an increase in charge transfer resistance (Rct) and polarization resistance (Rc), alongside a decrease in the constant phase element (CPE)—is commonly interpreted as evidence of a protective surface layer that impedes ionic transport and enhances corrosion resistance. However, alternative interpretations must be critically evaluated, including changes in material porosity that alter ionic pathways, variations in water uptake kinetics that affect measured impedance, or substrate modifications induced by environmental or mechanical stressors, all of which can mimic passive film behavior. Despite these possibilities, the passive film interpretation is frequently favored due to its consistent observation across corrosion studies, strong correlational evidence linking impedance trends to known passive film characteristics (e.g., thickness and composition), and its foundation in well-established electrochemical mechanisms describing oxide or protective layer formation. Thus, while alternative explanations warrant consideration, the convergence of empirical data with theoretical frameworks often provides robust support for passive film formation as the dominant phenomenon [51-55].

In this sample, the resistance values of the coating system, the charge transfer resistance, and its decreasing trend with the passage of time are improved as compared to EPGSi-7% sample. In fact, by increasing the shell polymer solution concentration from 7 to 10 wt. %, the diameter of the core-shell fibers increased, the amount of self-healing material loading increased, and finally, a greater self-healing process was carried out.

Fig. 13 shows the EIS curves of the scratched EPGSi-15% sample at different immersion times. After 24 hours of immersion, the impedance value at low frequencies has shown five times decrease compared to the sample without scratches. Nevertheless, after 36 hours, the diameter of the semicircle of the capacitive loop in the Nyquist curve has become larger and the capacitive behavior has appeared in a larger range compared to 24 hours. The phase angle has increased significantly compared to the time of 24 hours, and the breakdown frequency has moved significantly to lower frequencies (bode-phase curve). All these samples indicate the ability of active repair for self-healing coatings after the initial damage. Self-healing materials have prevented the diffusion of the corrosive environment into the coating and have led to the improvement of the protective performance of the coating system. With the further increase of the immersion time, the impedance values in low frequencies have been continuously decreasing. This behavior is in good agreement with the reduction of the diameter of the Nyquist semicircle and the reduction of the phase angle. However, in the EPGSi-15% sample compared to the EPGSi-7% and EPGSi-10%, the magnitude of the

impedance is higher at all immersion times, and the rate of impedance reduction is low. In such a way, after 16 days of immersion, the maximum impedance value at low frequencies of the scratched EPGSi-15% sample is equal to 1.39×10^{8} Ω.cm^2 which is three times more than the scratched EPGSi-10% sample (4.26×10^{4} Ω .cm^2) under the same conditions. In fact, in the EPGSi-15% sample, due to the higher concentration and deposition of core-shell fibers with a more uniform distribution, it is possible to load more and better self-healing material, which leads to better self-healing and increases the barrier properties as a result of the formation of the passive layer. The data in Table 6 show a good agreement between the values obtained by fitting the impedance curves at different immersion times. The values of R_c and R_{ct} after 36 hours, in comparision to 24 hours, increased. Increasing R_c and R_{ct} indicates the formation of a passive film at the interface of the metal and coating layer, which can affect the adhesion of the epoxy coating to improve the surface of the metal and prevent the cathodic delamination of the coating, and limits the diffusion of corrosion products under the coating. There is no significant difference in the increase of the capacitor capacitance of the coating and the double layer capacitor capacitance, which shows the diffusion of water in the coating, is the lowest and the passive film has limited the access of the corrosive electrolyte to the active sites on the surface of the steel substrate. Cathodic and anodic reactions have occurred in the presence of the passive film at the lower level and have resulted in lower corrosion products under the coating [56-58].

The results related to the data obtained from the fitting curves of the EIS plots in this case also show in Figs.14 that the increase of electrochemical corrosion reactions at the metal-coating interface with the decrease of R_c and R_{ct} and the increase of CPE_c and CPE_{dl} with the increase of immersion time. In fact, after creating a scratch, the self-healing process occurred in the first 24 hours of immersion. But with the increasing immersion time, the resistance value of the coating system at low frequencies has a sharp drop, and the capacitor capacity of the coating system has increased sharply. In the EPGSi-7% sample, since a PVA polymer solution with a low concentration was used to form the shell in the core-shell fibers, and according to the morphological investigations carried out in this case, the diameter of the core-shell fibers had the lowest amount, and as a result, a lower amount of self-healing material was loaded, and a weaker self-healing process was observed in this case compared to 10 and 15 wt. %.

So, by increasing the shell polymer solution concentration from 7 to 10 wt. %, the diameter of the core-shell fibers increased, the amount of self-healing material loading increased, and finally, a greater self-healing process was performed than EPGSi-7%. In the EPGSi-15%

sample, compared to the EPGSi-7% and EPGSi-10% samples, the magnitude of the coating resistance is higher in all immersion times and the rate of resistance decrease with the passage of time is lower. In such a way that after 16 days of immersion, the resistance of the scratched sample coating system in the EPGSi-15% sample is equal to 1.39×10^{8} $\Omega.cm^2$, which is lower than the resistance value in the EPGSi-10% sample (4.26×10^{4} $\Omega.cm^2$) at the same time is three times larger. Furthermore, in the EPGSi-15% sample, due to the higher concentration and the deposition of core-shell fibers with a more uniform distribution, it is possible to load more and better self-healing material, which leads to the better self-healing, increasing the barrier property and formation of the passive layer at the metal-coating system interface. The amount of CPE_{dl} in nanocomposite coatings containing core-shell fibers in the EPGSi-15% sample after 148 days is the lowest compared to EPGSi-7% and EPGSi-10% samples, which shows the better protective performance of nanocomposite coatings containing core-shell fibers on it. The change process of R_{ct} is in accordance with R_c, with the difference that R_{ct} is related to the state of the metal-coating interface, such as the separation of the interface, the compression of corrosion products or the formation of passive films in the interface.

The release kinetics of self-healing agents encapsulated within polyvinyl alcohol (PVA) shells are profoundly influenced by the concentration of PVA, which governs shell morphology, thickness, and permeability factors that collectively dictate the rate and efficiency of agent release [59-60].

Higher PVA concentrations typically yield thicker, less porous shells that impede molecular diffusion, whereas lower concentrations produce more permeable and porous structures that facilitate faster release; this relationship was empirically validated by Mizrahi et al. (2025), who observed an inverse correlation between PVA concentration and healing agent release rate from microcapsules. While mechanical damage such as scratches, cracks, or other forms of stress-induced fracture remains the primary trigger for agent release by rupturing the shell and exposing its contents, additional stimuli can significantly modulate the release process [61]. Environmental factors, including variations in pH and temperature, alter the solubility and swelling behavior of PVA, thereby influencing diffusion dynamics; for instance, Liu et al. [62] demonstrated that elevated temperatures enhanced the release of healing agents from PVA-based microcapsules.

Similarly, mechanical stress beyond simple scratching such as bending, compression, or cyclic loading can also induce shell failure and promote agent liberation, as evidenced by Wei et al. [63] who reported increased release under repeated loading conditions. Critically,

the synergistic interplay between mechanical and environmental stimuli enables the design of multi-responsive, dual-triggered self-healing systems that offer superior adaptability and healing performance in complex service environments.

In fact, with the increase in the concentration of the PVA polymer solution of the shell related to the core-shell fibers, the diameter of the shell has increased and more healable materials are loaded in core-shell fibers and the penetration of corrosive solution and electrochemical reactions of corrosion in the scratch area have been prevented [41-42]. Based on the results of electrochemical impedance spectroscopy and surface examination of the scratched area, it can be concluded that the composite coating system containing core-shell fibers, which is made of 15 wt. % PVA solution for electrospinning, has better self-healing and protection performance than other samples. The digital camera images of the surface area of composite coating samples containing core-shell fibers with 7, 10, and 15 wt. % concentrations of PVA shell after the salt spray test are presented in Fig. 15. The first signs of rust appeared after 48h, while there were no signs for samples with 15 wt. %. The first signs of blistering in the scratch area appeared for the sample with a concentration of 7 wt. % of PVA after 144 hours of the salt fog test, and the intensity of rusting is greater than in the sample with a concentration of 10 wt. %. After 168 hours, the initial blisters started to grow for the sample with a concentration of 7 wt. %, while for the sample with a concentration of 10 wt. %, a few blisters have been formed on the surface of the scratched area. Over time of the salt spray test, blisters grow in the scratched area, and at 264 hours, blisters appeared in other areas of the sample with a concentration of 7 wt. %, while in the sample with a concentration of 15 wt. %, there were no blisters and corrosion products. In addition, the intensity of corrosion products and rusted areas in the scratch area and its surroundings in the sample with 7 wt. % concentration has grown at a higher rate than the sample with 10 wt. % concentration and reached its highest level after 384 hours. It is no significant difference after 408 to 480 hours. Investigation of the images of the core-shell fiber morphology increased in the shell polymer solution concentration, the diameter of the fibers increases, and the loading rate of the self-healing core material increased. Therefore, there is a possibility of higher loading of repair material and the self-healing process, and this is the reason for the fewer corrosion products on the surface of the scratched area of the 15 wt. % samples [66-67].

3.3.3. Investigation the morphology of the scratched area

In Fig. 16, the morphology of the scratch area of the samples containing electrospun core-shell fibers in different concentrations of 7, 10, and 15 wt. % PVA as a shell was investigated using FE-SEM. As it has been observed, on the surface of the coating containing core-shell

fibers with a concentration of 7 wt. % shell, the scratched area has been healed to a small extent, and some corrosion products can be seen in the areas around the scratch (Fig. 16A1). By increasing the concentration of the polymer shell to 10 wt. %, the scratch area has been partially healed, and the edges of the scratch area on the left side do not show any traces of corrosion products and roughness (Fig. 16B1). In the sample containing core-shell fibers with a concentration of 15 wt. % shell, no traces of corrosion and corrosion products were observed on both sides of the edges of the scratched area, and the scratched area was completely healed (Fig. 16C1). Qualitative EDAX analysis taken from the surface of the scratched area of these samples shows the presence of more silicon element released from the polydimethylsiloxane core material in the scratched area with 15 wt. % concentration. According to Fig. 15 in the scratched area of the sample containing core-shell fibers in the concentration of 7, 10, and 15 wt. %, the number of elements was summarized in Fig. 16 (A2, B2, and C2). As can be seen, with the increase in the concentration of the polyvinyl alcohol polymer shell from 7 to 10 and 15 wt. %, respectively, the weight percentage of oxygen and chlorine elements as active elements of the corrosive environment decreased, and the weight percentage of silicon and iron elements increased. It is the reason for improving the corrosion performance and self-healing of the coating.

If it is inferred from the examination of morphology related to coaxial electrospun core-shell fibers in different shell concentrations, with the increase of shell concentration, the diameter of core-shell fibers is gotten bigger than before, and the possibility of loading self-healing core materials and repairing the scratched area has increased with the time. It provides the release of polydimethylsiloxane material due to the dissolution of the PVA polymer material of the shell in contact with the aqueous solution. These results confirmed the electrochemical investigations of impedance spectroscopy and morphology of the scratch area after the salt spray test [68-69].

3.4. Structure and Mechanism of self-healing nanocomposite coating

The structure of epoxy-silanized graphene oxide nanocomposite coating system containing core-shell fibers is presented in Fig. 17. As can be seen, the coating system consists of three layers. The first layer is made of epoxy-silanized graphene oxide nanocomposite coating on the metal substrate, the second layer is core-shell fibers, polydimethylsiloxane-polyvinyl alcohol and the third layer is composed of epoxy- silanized graphene oxide nanocomposite coating. Fig. 18 shows the protection mechanism of the nanocomposite coating system containing core-shell fibers. When local corrosion occurs, regeneration and oxidation reactions take place and cause pH distribution in the cathodic and anodic areas. In the case of

local corrosion in organic coating systems, the damaged area of the organic coating can be the anode, and the undamaged area acts as the local cathode. The regeneration of oxygen in the cathodic areas leads to alkalization, which raises the pH value to above 5. Due to the pH changes in the damaged areas, self-healing materials inside the fibers are released through these polymer nanochannels. Silane compounds are one of the important materials that are used as repairing agents and forming protective films. Silane precursor has organic groups along with silicon, which tend to hydrolyze in the water environment. The hydrolysis reaction leads to cross-linking, which ultimately leads to the formation of a solid coating film. Such a feature shows the potential of this material as a repair agent in organic coatings. The self-healing mechanism of epoxy-silanized graphene oxide nanocomposite coating systems containing core-shell fibers, and polydimethylsiloxane-polyvinyl alcohol, due to the diffusion of the corrosive solution inside the coating system and contact with the core-shell fibers leads to the release of the polydimethylsiloxane polymer as a result of the dissolution of the hydrophilic polyvinyl alcohol polymer shell and a passive protective layer. That layer prevents further penetration of corrosive ions in the coating system. After diffusion of the aqueous solution into the coating, Si-OR groups are hydrolyzed and form Si-OH bonds. Moreover, in the following condensation reactions happened, other Si-O-Si and Si-O-C bonds are formed inside the coating. By the formation of these silane bonds in the epoxy polymer matrix, the density of the cross-link increases, and the diffusion paths of the electrolyte in the coating system are reduced [68-70].

In epoxy–graphene oxide nanocomposite systems incorporating core–shell nanofibers with polydimethylsiloxane (PDMS) as the core healing agent, a critical trade-off exists between mechanical performance and self-healing efficiency. While PDMS enhances self-healing due to its low surface energy, fluidity, and ability to flow into and seal microcracks, its incorporation can adversely affect key mechanical properties. Excessive PDMS content may reduce interfacial adhesion between the nanofibers and the epoxy matrix, compromising structural integrity under mechanical load, and can also lower the composite's overall hardness and stiffness—attributes essential for applications requiring rigidity and load-bearing capacity. Moreover, an overabundance of PDMS may impede healing kinetics by creating an overly soft or viscous network that hinders the efficient diffusion and distribution of the healing agent. The viscoelastic nature of PDMS further contributes to energy dissipation during crack propagation, which can be beneficial for damage tolerance but simultaneously diminishes elastic modulus and strength. Additionally, high PDMS loading can disrupt the uniform dispersion of graphene oxide—a key nanofiller that imparts strength

and stiffness—potentially leading to agglomeration and diminished reinforcement. Therefore, achieving an optimal balance between self-healing functionality and mechanical robustness requires precise control over PDMS concentration. Systematic evaluation of varying PDMS loadings, with concurrent assessment of mechanical properties (e.g., adhesion, hardness, stiffness) and healing efficiency, is essential to identify a formulation that satisfies the dual demands of structural performance and autonomous repair in targeted applications [71-73].

4. Conclusion

In this research, a coating system resistant to corrosive environment and self-healing was produced with the polydimethylsiloxane-polyvinyl alcohol core-shell nanofibers in epoxy-silanized graphene oxide nanocomposite coating. The morphological investigations of core-shell fibers were conducted with using TEM, FE-SEM and fluorescent microscope analysis in order to determine the optimum condition. So the silane epoxy-graphene oxide coating containing electrospun core-shell fibers with 15 wt. % PVA solution was selected as the optimal sample. The EIS test was used to investigate the protective and self-healing performance of the nanocomposite coating system containing core-shell fibers. Also, the salt spray test was performed on the coated steel substrates and the surface of the scratched area exposed to the accelerated corrosive environment was checked with the help of FE-SEM microscope and EDAX analyzer. The existence of self-healing properties due to the release of core materials from the core-shell fibers in the silane epoxy-graphene oxide nanocomposite coating system when the corrosive aqueous materials collide through the pores and cracks created in the coating during the immersion time causes the increase in the resistance of the coating system. The results of the high impedance resistance of the coating system after 148 days of immersion of the sample without scratches and 16 days of immersion of the sample with scratches indicate the excellent performance of corrosion resistance and self-healing of the nanocomposite coating system containing core-shell fibers.

The durability and longevity of the self-healing mechanism are critical factors governing its repeatability and long-term efficacy. Over time or with repeated activation, healing agents or the delivery infrastructure may degrade, potentially diminishing the material's capacity to heal effectively. Experimental evidence indicates that while many self-healing materials can undergo multiple healing cycles, they often exhibit diminishing returns in terms of recovered mechanical properties or barrier performance after each event, underscoring the need for systematic investigation into the cumulative effects of repeated healing. Vascular inspired systems offer a distinct advantage in this regard: by mimicking biological circulatory networks, they enable theoretically unlimited healing cycles, provided the fibrous or channel-

based network remains intact and functional. Their interconnected architecture facilitates a dynamic and distributed response to damage allowing healing agents to be rerouted through undamaged pathways to reach affected regions, thereby ensuring adaptability and resilience. In contrast, capsule based systems are inherently limited by the finite number of pre-embedded microcapsules, supporting only a fixed number of localized healing events without the possibility of replenishment or network level adaptation. Consequently, vascular systems not only enhance repeatability but also provide a more robust and responsive framework for long-term corrosion protection or structural self-repair in advanced coating technologies.

Funding

The implementers of this project have received a grant from Iran National Science Foundation (INSF)

Acknowledgements

The authors of this research consider it necessary to appreciate the support of the Iran National Science Foundation (INSF), who helped us in carrying out this research.

Data availability

Data use support the finding of this study are available from corresponding author upon reasonable request**.**

Refrence

[1] AM. Atta, HA. Al-Lohedan, AM. El-saeed, HI. Al-Shafey, MH. Wahby, Epoxy embedded with TiO_2 nanogel composites as promising self-healing organic coatings of steel, Prog. Org. Coat., 105 (2017) 291-302. https://doi.org/10.1016/j.porgcoat.2017.01.009.

[2] MD. Tomić, B. Dunjić, V. Likić, J. Bajat, J. Rogan, Branko Dunjić, J. Djonlagić, J. Djonlagić, The use of nanoclay in preparation of epoxy anticorrosive coatings, Prog. Org. Coat., 77, no. 2 (2014) 518-527. https://doi.org/10.1016/j.porgcoat.2013.11.017.

[3] F. Cotting, IV. Aoki, Smart protection provided by epoxy clear coating doped with polystyrene microcapsules containing silanol and Ce (III) ions as corrosion inhibitors, Surf. Coat. Tech*.,* 303 (2016) 310-318. https://doi.org/10.1016/j.surfcoat.2015.11.035.

[4] H. Vakili, B. Ramezanzadeh, R. Amini, The corrosion performance and adhesion properties of the epoxy coating applied on the steel substrates treated by cerium-based conversion coatings, Corr. Sci. 94 (2015) 466-475. https://doi.org/10.1016/j.corsci.2015.02.028.

[5] V. Dalmoro, C. Alemán, CA. Ferreira, J.HZ. Dos Santos, D.S. Azambuja, E. Armelin, The influence of organophosphonic acid and conducting polymer on the adhesion and protection of epoxy coating on aluminium alloy, Prog. Org. Coat., 88 (2015) 181-190. https://doi.org/10.1016/j.porgcoat.2015.07.004.

[6] Zhang, Hao, Hao Yu, Chang Liu, Yesheng Huang, Haoyu Wu, Pan Yi, Kui Xiao, and Jin Gao. "Mechanistic Investigation of the Corrosion Behavior of Organic Zn14Al1. 4 Composite Coating Under Simulated Tropical Marine Atmospheric Conditions." Coatings 15, no. 9 (2025): 981.

[7] Ma, Qingyun, Qing Yang, Jialiang Zhang, Fangzheng Ren, Chongxiao Xia, and Feng Chen. "Anti-corrosion properties of bio-inspired surfaces: a systematic review of recent research developments." Materials Advances 5, no. 7 (2024): 2689-2718.

[8] RS. Trask, HR. Williams, IP. Bond, Self-healing polymer composites: mimicking nature to enhance performance, Bioinspir. Biomim, 2, no. 1 (2007) P1. DOI 10.1088/1748-3182/2/1/P01.

[9] DY. Wu, S. Meure, D. Solomon, Self-healing polymeric materials: A review of recent developments, Prog. Polym. Sci. 33, no. 5 (2008) 479-522. https://doi.org/10.1016/j.progpolymsci.2008.02.001.

[10] ML. Zheludkevich, J. Tedim, MGS. Ferreira, Smart coatings for active corrosion protection based on multi-functional micro and nanocontainers, Electrochim. Acta, 82 (2012) 314-323. https://doi.org/10.1016/j.electacta.2012.04.095.

[11] MF. Montemor, Functional and smart coatings for corrosion protection: A review of recent advances, Surf. Coat. Tech., 258 (2014) 17-37. https://doi.org/10.1016/j.surfcoat.2014.06.031.

[12] M. Plawecka, D. Snihirova, B. Martins, K. Szczepanowicz, P. Warszynski, MF. Montemor, Self-healing ability of inhibitor-containing nanocapsules loaded in epoxy coatings applied on aluminium 5083 and galvanneal substrates, Electrochim. Acta, 140 (2014) 282-293. https://doi.org/10.1016/j.electacta.2014.04.035.

[13] C. Zotiadis, I. Patrikalos, V. Loukaidou, DM. Korres, A. Karantonis, S. Vouyiouka, Self-healing coatings based on poly (urea-formaldehyde) microcapsules: In situ polymerization, capsule properties and application, Prog. Org. Coat., 161 (2021) 106475. https://doi.org/10.1016/j.porgcoat.2021.106475.

[14] A. Fereidoon, M. G. Ahangari, M. Jahanshahi, Effect of nanoparticles on the morphology and thermal properties of self-healing poly (urea-formaldehyde) microcapsules, J. Polym. Res, 20 (2013) 1-8. https://doi.org/10.1007/s10965-013-0151-3.

[15] E. Koh, NK. Kim, J. Shin, YW. Kim, Polyurethane microcapsules for self-healing paint coatings, RSC. Adv., 4, no. 31 (2014) 16214-16223. https://doi.org/10.1039/C4RA00213J.

[16] AR. Hamilton, NR. Sottos, SR. White, Pressurized vascular systems for self-healing materials, J. R. Soc. Interface.,9, no. 70 (2012): 1020-1028. https://doi.org/10.1098/rsif.2011.0508.

[17] JH. Park, PV. Braun,Coaxial electrospinning of self-healing coatings, Adv. Mater., 22, no. 4 (2010) 496-499. DOI: 10.1002/adma.200902465.

[18] C. Wang, KW. Yan, YD. Lin, PCH. Hsieh, Biodegradable core/shell fibers by coaxial electrospinning: processing, fiber characterization, and its application in sustained drug release, Macromolecules, 43, no. 15 (2010) 6389-6397. https://doi.org/10.1021/ma100423x.

[19] H. Zhang, P. Wang, J. Yang, Self-healing epoxy via epoxy–amine chemistry in dual hollow glass bubbles, Compos. Sci. Technol., 94 (2014) 23-29. https://doi.org/10.1016/j.compscitech.2014.01.009.

[20] DG. Bekas, D. Baltzis, AS. Paipetis ,Nano-reinforced polymeric healing agents for vascular self-repairing composites, Mater. Des, 116 (2017) 538-544. https://doi.org/10.1016/j.matdes.2016.12.049.

[21] TQ. Doan, LS. Leslie, SY. Kim, R. Bhargava, SR. White, NR. Sottos, Characterization of core-shell microstructure and self-healing performance of electrospun fiber coatings, Polymer, 107 (2016) 263-272. https://doi.org/10.1016/j.polymer.2016.10.062.

[22] P. Li, Z. Shang, K. Cui, H. Zhang, Z. Qiao, C. Zhu, N. Zhao, J. Xu, electrospinning core-shell fibers for self-healing scratch on coatings, Chin. Chem. Lett, 30, no. 1 (2019) 157-159. https://doi.org/10.1016/j.cclet.2018.01.037.

[23] MW. Lee, S. An, C. Lee, M. Liou, AL. Yarin, SS. Yoon ,Hybrid self-healing matrix using core–shell nanofibers and capsuleless microdroplets, ACS. Appl. Mater. Interfaces, 6, no. 13 (2014) 10461-10468.

[24] MW. Lee, S. An, HS. Jo, SS. Yoon, AL. Yarin, Self-healing nanofiber-reinforced polymer composites. 1. Tensile testing and recovery of mechanical properties, ACS. Appl. Mater. Interfaces, 7, no. 35 (2015) 19546-19554.

[25] MW. Lee, S. An, HS. Jo, SS. Yoon, AL. Yarin, Self-healing nanofiber-reinforced polymer composites. 2. Delamination/debonding and adhesive and cohesive properties, ACS. Appl. Mater. Interfaces, 7, no. 35 (2015) 19555-19561.

[26] Putra, Nicky Rahmana, Sahlan Sahlan, Wibowo Harso Nugroho, Widodo Widodo, Ahmad Syafi'ul Mujahid, Afian Kasharjanto, Mochamad Saiful, Lailatul Qomariyah, and

Irianto Irianto. "Natural sustainable coatings for marine applications: advances, challenges, and future perspectives." *Green Processing and Synthesis* 14, no. 1 (2025): 20250035.

[27] Sazali, Nur Hidayah, Siti Nur Syazni Mohd Zuki, Noorhaslin Che Su, Sofyah Anis Izwani Jusof, Abdul Hazim Abdullah, Chee Sheau Chien, and Mohd Azuwan Maoinser. "A Review on Self-Healing Coatings Technologies for Sustainable and Resilient Surfaces." In Offshore Technology Conference, p. D031S039R003. OTC, 2025.

[28] Srivastav, Ruchir Shanker, and Aarti P. More. "A Comprehensive Review of Self-Healing Polymers: Mechanisms, Types, and Industry Implications." Polymers for Advanced Technologies 36, no. 2 (2025): e70092.

[29] Vu, Nhu Q., Thai M. Le, An NB Ngo, Minh HT Nguyen, Ying-Chih Liao, and Thuy T. Tran. "Engineering Functional PVA: A Comprehensive Review of Chemical Modifications and Prospective Developments." ACS Polymers Au (2025).

[30] Akhila, B., V. Abhijith, Mridula Sreedharan, Lakshmipriya Ravindran, Aiswarya Sathian, Sabu Thomas, and Sreekala Meyyarappallil Sadasivan. "Innovations in Core–Shell Electrospinning: A Comprehensive Review in Recent Advances of Core–Shell Electrospun Polylactic Acid Nanocomposite Fibers for Potential Biomedical Applications." ACS Biomaterials Science & Engineering (2025).

[31] Yadav, Sandeep Kumar, Vishwa Prakash Jha, Durga Prasad Pabba, and Arun Thirumurugan. "Development of Core-Shell Nanofibers in Magnetoelectric Sensors, Fuel Cells, and Drug-Delivery Applications: A Review." Sustainable Energy & Fuels (2026).

[32] Wang, Shuo, Ruifan Wang, Xinran Zhang, Yucheng Li, and Hao Ma. "Engineering core–sheath phase change fibers for thermal energy storage: fundamentals, fabrication, and smart applications." Journal of Materials Chemistry A 13, no. 45 (2025): 38668-38702.

[33] S. M. Madani, P. Sangpour, M. R. Vaezi, B. Ramezanzadeh, M. Amani-Tehran, Organosilane-functionalized graphene oxideepoxy nanocomposite coating: corrosion performance and self-healing properties, Surf. Topogr. Metrol. Prop. 10 (2022) 035002.

[34] HS. Mansur, CM. Sadahira, AN. Souza, AAP. Mansur, FTIR spectroscopy characterization of poly (vinyl alcohol) hydrogel with different hydrolysis degree and chemically crosslinked with glutaraldehyde, Mater. Sci. Eng. C, 28, no. 4 (2008) 539-548. https://doi.org/10.1016/j.msec.2007.10.088.

[35] MW. Keller, SR. White, NR. Sottos, A self-healing poly (dimethyl siloxane) elastomer, Adv. Funct. Mater, 17, no. 14 (2007) 2399-2404.

[36] A. Haider, S. Haider, IK. Kang, A comprehensive review summarizing the effect of electrospinning parameters and potential applications of nanofibers in biomedical and biotechnology, Arab. J. Chem, 11, no. 8 (2018) 1165-1188. https://doi.org/10.1016/j.arabjc.2015.11.015.

[37] V. Pillay, C. Dott, YE. Choonara, C. Tyagi, L. Tomar, P. Kumar, LC. du Toit, VMK. Ndesendo, A review of the effect of processing variables on the fabrication of electrospun nanofibers for drug delivery applications, J. Mater, no. 1 (2013): 789289.

[38] X. Wang, W. Xing, P. Zhang, L. Song, H. Yang, Y. Hu Wang, Covalent functionalization of graphene with organosilane and its use as a reinforcement in epoxy composites, Compos. Sci. Technol, 72, no. 6 (2012) 737-743. https://doi.org/10.1016/j.compscitech.2012.01.027.

[39] YJ. Wan, LX. Gong, LC. Tang, LB. Wu, JX. Jiang Wan, Mechanical properties of epoxy composites filled with silane-functionalized graphene oxide, Compos. Part A. Appl. Sci. Manuf, 64 (2014) 79-89. https://doi.org/10.1016/j.compositesa.2014.04.023.

[40] SK. Yadav, JW. Cho, Functionalized graphene nanoplatelets for enhanced mechanical and thermal properties of polyurethane nanocomposites. Appl. Surf. Sci, 266 (2013) 360-367. https://doi.org/10.1016/j.apsusc.2012.12.028.

[41] JK. Park, DS. Kim, Effects of an aminosilane and a tetra functional epoxy on the physical properties of difunctional epoxy/graphene nanoplatelets nanocomposites, Polym. Eng. Sci, 54, no. 4 (2014) 969-976.

[42] S. Sinha-Ray, DD. Pelot, ZP. Zhou, A. Rahman, XF. Wu, AL. Yarin, Encapsulation of self-healing materials by coelectrospinning, emulsion electrospinning, solution blowing and intercalation, J. Mater. Chem, 22, no. 18 (2012) 9138-9146. https://doi.org/10.1039/C2JM15696B.

[43] XF. Wu, A. Rahman, Z. Zhou, DD. Pelot, S. Sinha-Ray, B. Chen, S. Payne, AL. Yarin , Electrospinning core-shell nanofibers for interfacial toughening and self-healing of carbon fiber/epoxy composites, J. Appl. Polym. Sci, 129, no. 3 (2013) 1383-1393. https://doi.org/10.1002/app.38838.

[44] Y. Dong, S. Li, Q. Zhou, Self-healing capability of inhibitor-encapsulating polyvinyl alcohol/polyvinylidene fluoride coaxial nanofibers loaded in epoxy resin coatings, Prog. Org. Coat, 120 (2018) 49-57. https://doi.org/10.1016/j.porgcoat.2018.03.010.

[45] J. Cui, Z. Xiong, H. Qiu, LI. Jing, J. Yang Cui, Functionalized graphene oxide: Carrier for corrosion inhibitor and barrier in waterborne epoxy coatings, Compos. **Part** A. Appl. Sci. Manuf, 144 (2021) 106354. https://doi.org/10.1016/j.compositesa.2021.106354.

[46] Paul, Sudipta, Ankit Kumar Kaushik, Amul Jain, and Sanjib Banerjee. "Intelligent self-healing polymeric systems for functional and durable coatings." *Chemistry–An Asian Journal* (2025): e70290.

[47] Chatterjee, Amrita, Agrima Yadav, Sushmit Sen, Sourav Ghosh, Nitesh Choudhary, Nilanjan Dey, Sunidhi Mishra, and Pradip K. Maji. "Polymer-modified nonwovens: functional surfaces for separation, sensing, biomedical and smart textile applications." Journal of Materials Chemistry A (2026).

[48] Cao, Mingmei, Mohan Li, Quan Zhou, Jinsong Rao, and Yuxin Zhang. "The active corrosion protection of layered double hydroxides inhibitor nanocontainers: a review." Journal of Materials Science (2025): 1-23.

[49] Paul, Sudipta, Ankit Kumar Kaushik, Amul Jain, and Sanjib Banerjee. "Intelligent self-healing polymeric systems for functional and durable coatings." Chemistry–An Asian Journal (2025): e70290.

[50] Y. Ye, D Zhang, T. Liu, Z. Liu, W. Liu, J. Pu, H. Chen, H. Zhao, X. LiYe, Improvement of anticorrosion ability of epoxy matrix in simulate marine environment by filled with superhydrophobic POSS-GO nanosheets, J. Hazard. Mater, 364 (2019) 244-255. https://doi.org/10.1016/j.jhazmat.2018.10.040.

[51] Hoque, Md Ashraful, and Chun-Wei Yao. "Nanoscale Characterization of Nanomaterial-Based Systems: Mechanisms, Experimental Methods, and Challenges in Probing Corrosion, Mechanical, and Tribological Properties." Nanomaterials 15, no. 23 (2025): 1824.

[52] Srivastav, Ruchir Shanker, and Aarti P. More. "A Comprehensive Review of Self-Healing Polymers: Mechanisms, Types, and Industry Implications." Polymers for Advanced Technologies 36, no. 2 (2025): e70092.

[53] Kashef Tabrizian, Seyedreza, Seppe Terryn, and Bram Vanderborght. "Toward Autonomous Self-Healing in Soft Robotics: A Review and Perspective for Future Research." Advanced Intelligent Systems (2025): 2400790.

[54] Liu, Xiaodong. "Review of protective coatings for corrosion mitigation in chemical machinery: performance and mechanical aspects." Journal of Adhesion Science and Technology (2025): 1-50.

[55] Zhao, Xin, Huiru Xu, Yuchen Sun, Yutong Yang, and Baolin Guo. "Self-Adaptive Wound Dressings for Wound Healing and Repair." Advanced Materials (2025): e15854.

[56] X. Zhu, Z. Ni, L. Dong, Z. Yang, L. Cheng, X. Zhou, Y. Xing, J. Wen, M. Chen, In-situ modulation of interactions between polyaniline and graphene oxide films to develop

waterborne epoxy anticorrosion coatings, Prog. Org. Coat, 133 (2019) 106-116. https://doi.org/10.1016/j.porgcoat.2019.04.016.

[57] B. Ramezanzadeh, G. Bahlakeh, M. Ramezanzadeh, Polyaniline-cerium oxide (PAni-CeO_2) coated graphene oxide for enhancement of epoxy coating corrosion protection performance on mild steel, Corros. Sci, 137 (2018) 111-126. https://doi.org/10.1016/j.corsci.2018.03.038.

[58] N. Parhizkar, B. Ramezanzadeh, T. Shahrabi, The epoxy coating interfacial adhesion and corrosion protection properties enhancement through deposition of cerium oxide nanofilm modified by graphene oxide, J. Ind. Eng. Chem, 64 (2018) 402-419. https://doi.org/10.1016/j.jiec.2018.04.003.

[59] Pastrafidou, Maria, Evangelia C. Vouvoudi, Vassilios Binas, and Ioannis A. Kartsonakis. "Superabsorbent Core/Shell Composite Materials: A Review on Synthesis, Design and Applications." Polymers 17, no. 11 (2025): 1461.

[60] Filimon, Anca, Adina Maria Dobos, Mihaela Dorina Onofrei, and Diana Serbezeanu. "Polyvinyl Alcohol-Based Membranes: A Review of Research Progress on Design and Predictive Modeling of Properties for Targeted Application." Polymers 17, no. 8 (2025): 1016.

[61] Mizrahi, Limor, Rotem Kelman, Efrat Shtriker, David Meridor, Dror Cohen, Meital Portugal-Cohen, and Elizabeth Amir. "Controlled Release of Hydrophilic Active Agent from Textile Using Crosslinked Polyvinyl Alcohol Coatings." Journal of Functional Biomaterials 16, no. 6 (2025): 216.

[62] Liu, Zeying, Huixia Li, Yalin Huang, Jie Li, Ruiying Dong, Xue Yun, Yuqian Ren et al. "Thermal-responsive microgels incorporated PVA composite hydrogels: Integration of two-stage drug release and enhanced self-healing ability for chronic wound treatment." Chemical Engineering Journal 506 (2025): 159813.

[63] Wei, Zihao, Xiaomin Zhang, Tianqi Cao, Tian Luo, Yuanjing Sun, Zihan Jin, and Changhu Xue. "Fabrication of core–shell–shell nanoparticles as co-encapsulation systems via ultrasonic treatment optimization: Encapsulation performance and programmed sequential release analyses." Food Hydrocolloids 164 (2025): 111199.

[64] H. Yi, Y. Deng, C. Wang, Pickering emulsion-based fabrication of epoxy and amine microcapsules for dual core self-healing coating, Compos. Sci. Technol, 133 (2016) 51-59. https://doi.org/10.1016/j.compscitech.2016.07.022.

[65] S. An, M. Liou, KY. Song, HS. Jo, MW. Lee, SS. Al-Deyab, AL. Yarin, SS. Yoon,

Highly flexible transparent self-healing composite based on electrospun core–shell nanofibers produced by coaxial electrospinning for anti-corrosion and electrical insulation, Nanoscale 7, no. 42 (2015) 17778-17785. https://doi.org/10.1039/C5NR04551G.
[66] TJ. Mitchell, MW. Keller, Coaxial electrospun encapsulation of epoxy for use in self-healing materials, Polym. Int, 62, no. 6 (2013) 860-866. https://doi.org/10.1002/pi.4397
[67] H. Li, Y. Cui, H. Wang, Y. Zhu, B. Wang ,Preparation and application of polysulfone microcapsules containing tung oil in self-healing and self-lubricating epoxy coating, Colloids. Surf. A: Physicochem. Eng. Asp, 518 (2017) 181-187. https://doi.org/10.1016/j.colsurfa.2017.01.046.
[68] M. Kasaeian, E. Ghasemi, B. Ramezanzadeh, M. Mahdavian, G. Bahlakeh, Construction of a highly effective self-repair corrosion-resistant epoxy composite through impregnation of 1H-Benzimidazole corrosion inhibitor modified graphene oxide nanosheets (GO-BIM), Corros. Sci, 145 (2018) 119-134. https://doi.org/10.1016/j.corsci.2018.09.023.
[69] V. Vahedi, P. Pasbakhsh, CS. Piao, CE. Seng, A facile method for preparation of self-healing epoxy composites: using electrospun nanofibers as microchannels, J. Mater. Chem. A, 3, no. 31 (2015) 16005-16012. https://doi.org/10.1039/C5TA02294K.
[70] SM. Madani, M. Ehteshamzadeh, H. H. Rafsanjani ,2012, Surface Pre-treatment Coating Film and Process for Metallic Substrates, United States Patents, NO. 8273411.
[71] Ratwani, Chirag R., Kostya S. Novoselov, and Amr M. Abdelkader. "Applications and mechanistic insights into intrinsically self-healing polymers with multifunctional 2D materials." SusMat 5, no. 4 (2025): e70028.
[72] Cordoba, Aldo, Fabiola A. Gutiérrez-Mejía, Gabriel Cepeda-Granados, Juan V. Cauich-Rodríguez, and Karen Esquivel Escalante. "Self-Healing Polymer-Based Coatings: Mechanisms and Applications Across Protective and Biofunctional Interfaces." Polymers 17, no. 23 (2025): 3154.
[73]Yang, Manping, Shiyu Long, Junjie Gao, Jiang Han, Chao Yang, Luyao Shi, Daxin Zhou, and Bingfan Li. "Application and Challenges of Self-Healing Polymer Coatings in Metal Corrosion Protection." Materials and Corrosion (2025).

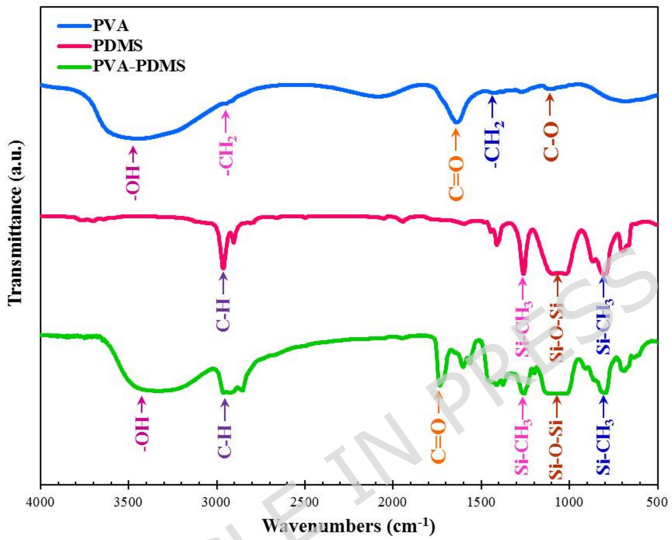

FIG. 1: The FTIR spectrums of polyvinyl alcohol (PVA) solution, polydimethylsiloxane (PDMS) solution and core-shell fibers (PVA-PDMS).

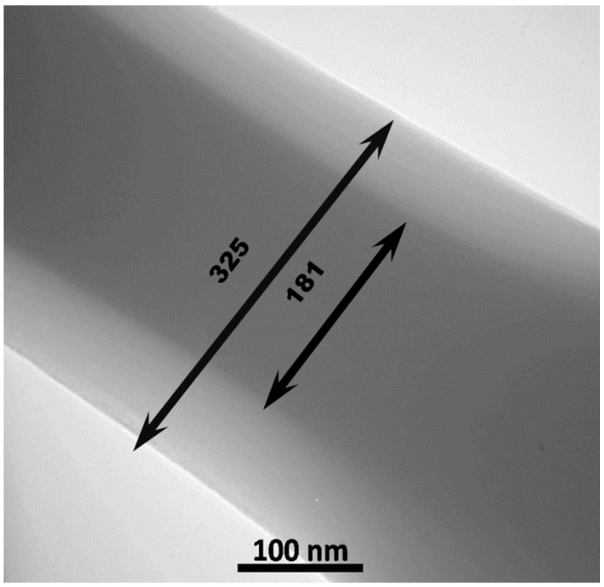

FIG. 2: TEM image of core-shell structure in PDMS-PVA nanofibers.

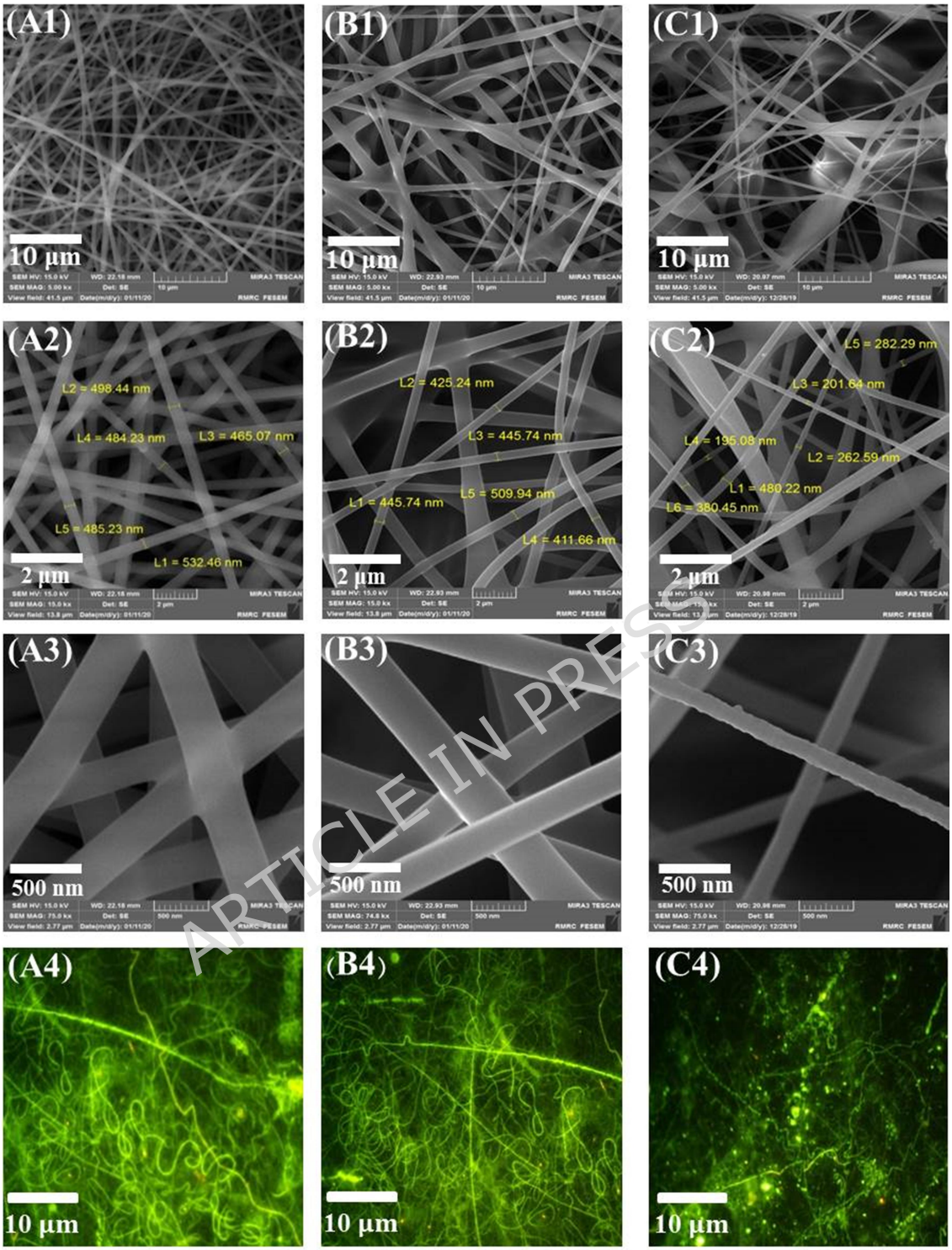

FIG. 3: The FE-SEM (A, B, C) and fluorescent microscope(D) images of electrospinning core-shell fibers at 13kV voltage, core feeding rate 0.2 $mL.h^{-1}$, distance 18 cm from the tip of the syringe needle to the collector, polymer solution 40 wt. % Polydimethyl siloxane (core), and different concentration of polyvinyl alcohol solution (shell); (A) 7, (B) 10 and (C) 15 wt. %

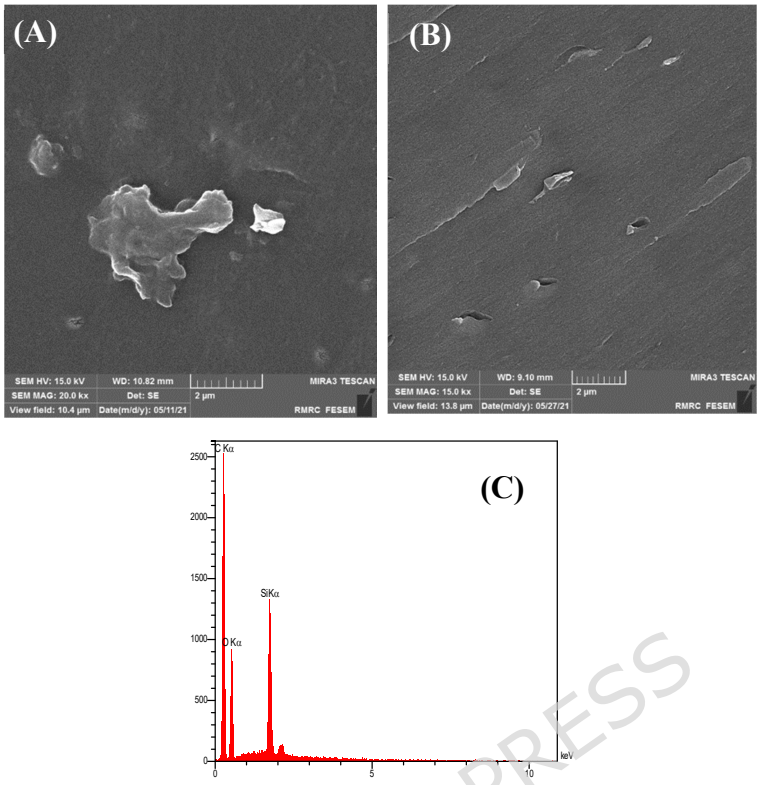

FIG. 4: The FE-SEM images of 0.2 wt. % epoxy composite coating of pure graphene oxide (A) and silane graphene oxide (B) along with EDS elemental analysis of the surface of epoxy-silane graphene oxide composite coating (C).

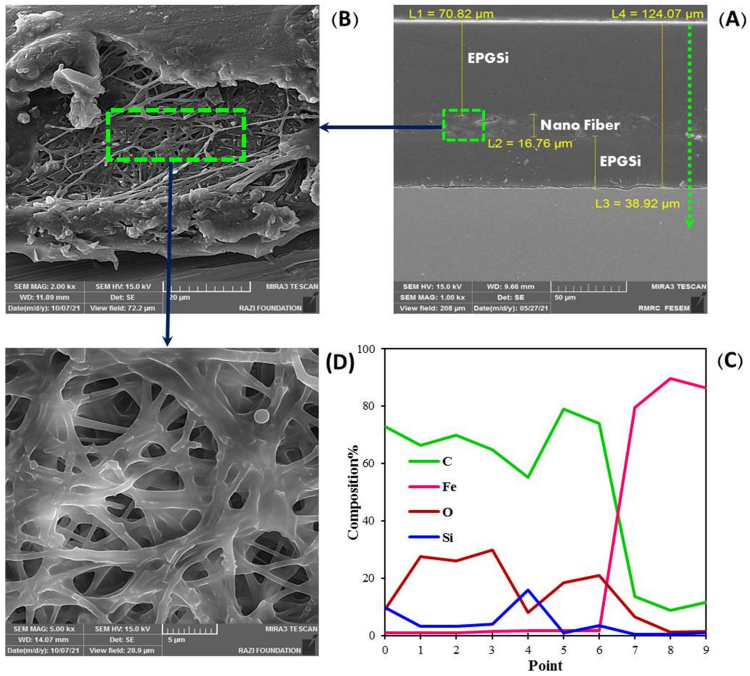

FIG. 5: The FE-SEM image of the cross-sectional surface of epoxy-silane graphene oxide coating containing core-shell fibers (A), the cross-sectional image of the middle layer of the coating system (B), the linear elemental EDS analysis along the green arrow and coating thickness (C) and the magnification of the middle layer of the coating system (D).

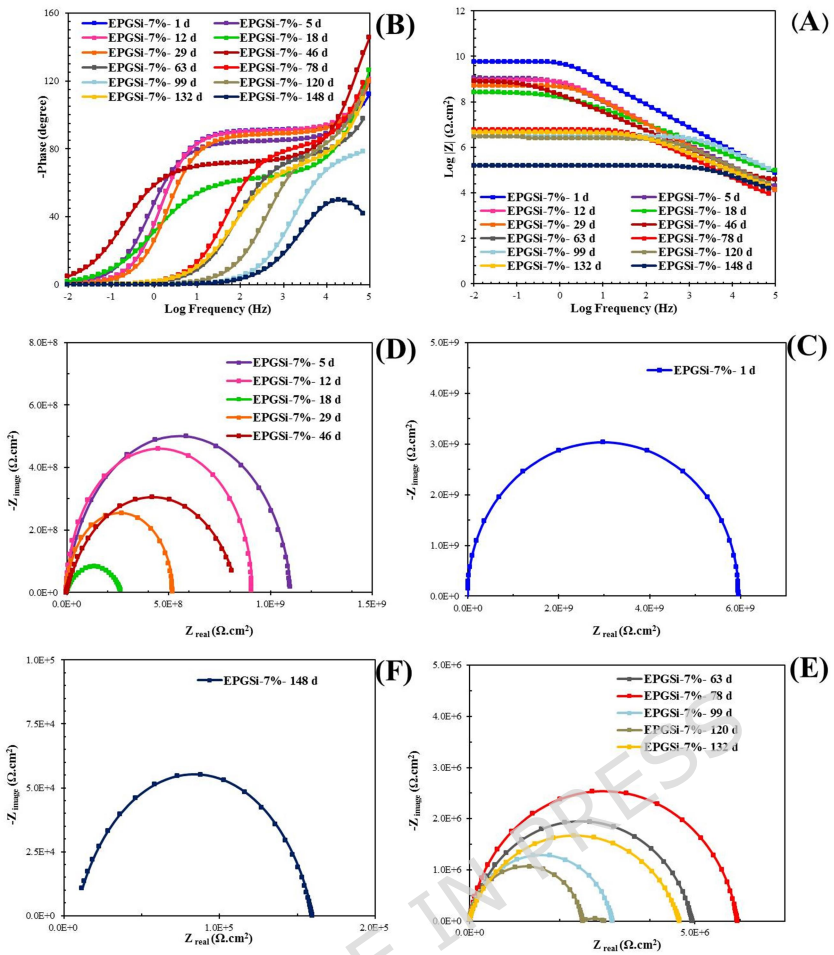

FIG. 6: The EIS curves of silane epoxy-graphene oxide coating containing electrospun core-shell fibers with 7 wt. % PVA solution (A) Bode curves from 1 to 148 days, (B) Bode-phase curves from 1 to 148 days, (C) Nyquist curve 1 day, (D) Nyquist curves 5, 12, 18, 29 and 46 days, (E) 63, 78, 99, 120 and 132 days and (F) 148 days immersion in 3.5 wt. % sodium chloride solution.

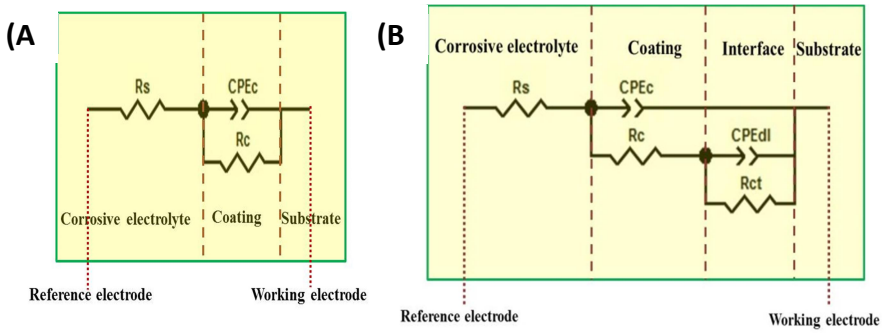

FIG. 7: Equivalent electrical circuit (EEC) of epoxy coating and composite epoxy-graphene oxide silanized in 3.5 wt. % sodium chloride solution in initial times (A) and long immersion times (B)

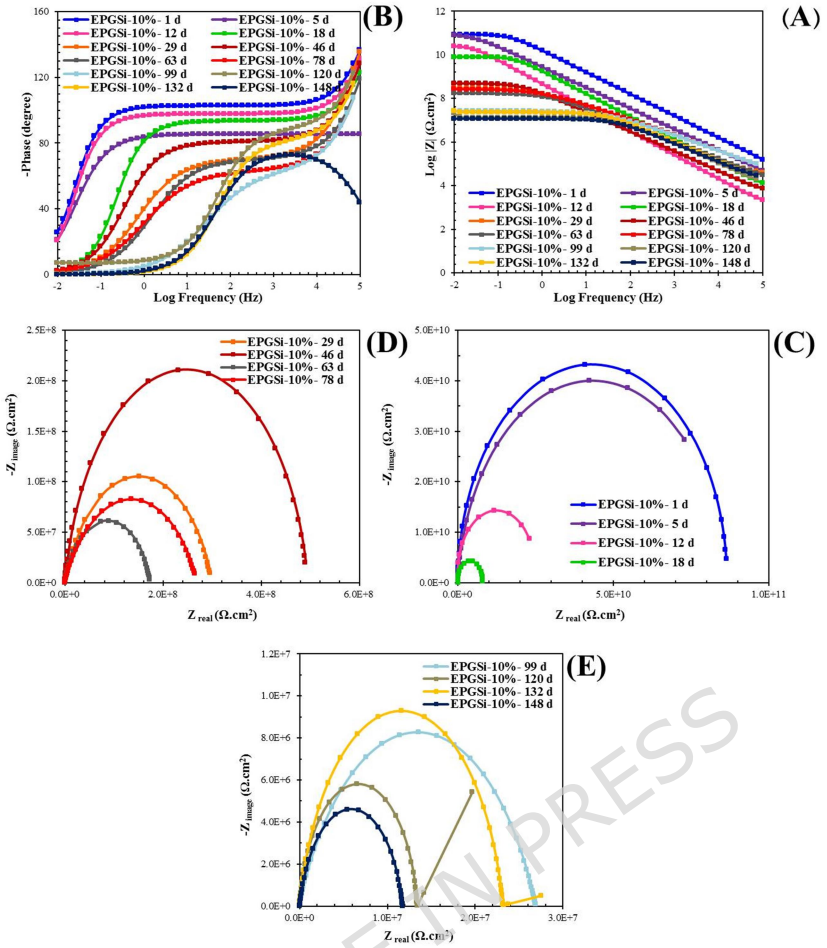

FIG. 8: The EIS curves of silane epoxy-graphene oxide coating containing electrospun core-shell fibers with 10 wt. % PVA solution (A) Bode curves from 1 to 148 days, (B) Bode-phase curves from 1 to 148 days, (C) Nyquist curves 1, 5, 12 and 18 days, (D) Nyquist curves 29, 46, 63 and 78 days (E) 99, 120, 132 and 148 days immersion in 3.5 wt. % sodium chloride solution.

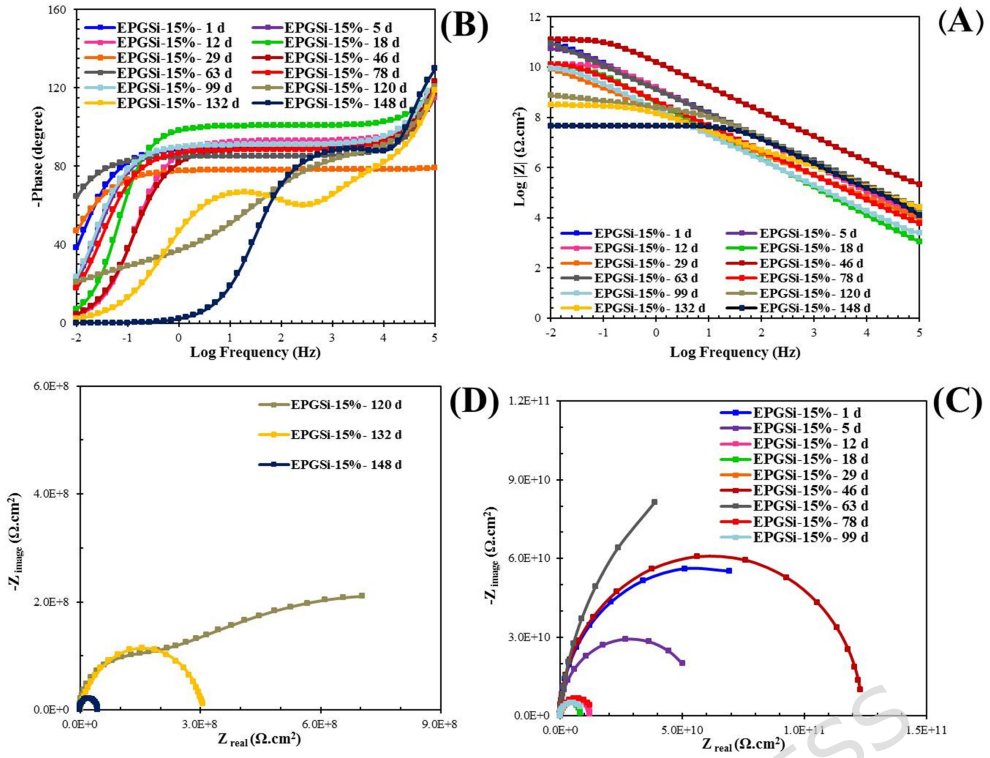

FIG. 9: The EIS curves of silane epoxy-graphene oxide coating containing electrospun core-shell fibers with 15 wt. % PVA solution (A) Bode curves from 1 to 148 days, (B) Bode-phase curves from 1 to 148 days, (C) Nyquist curves 1 to 99 days (D) Nyquist curves 120, 132 and 148 days immersion in 3.5 wt. % sodium chloride solution.

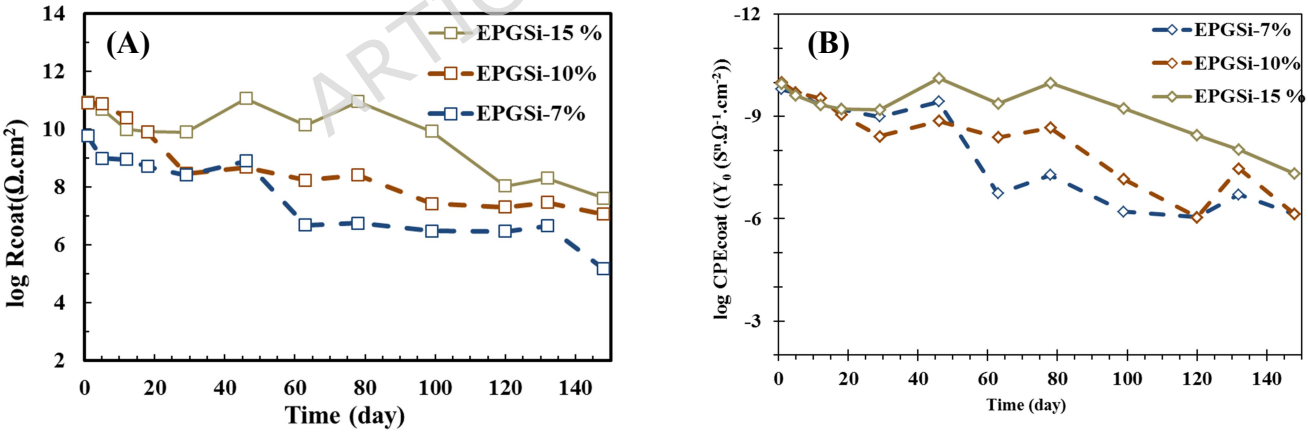

FIG. 10: The changes in coating resistance (A) and equivalent capacitance (B) of epoxy-silanized graphene oxide nanocomposite coating system containing electrospun core-shell fibers with PVA solution at concentrations of 7, 10 and 15 wt. % during 148 days of immersion in a solution of 3.5 wt. % sodium chloride.

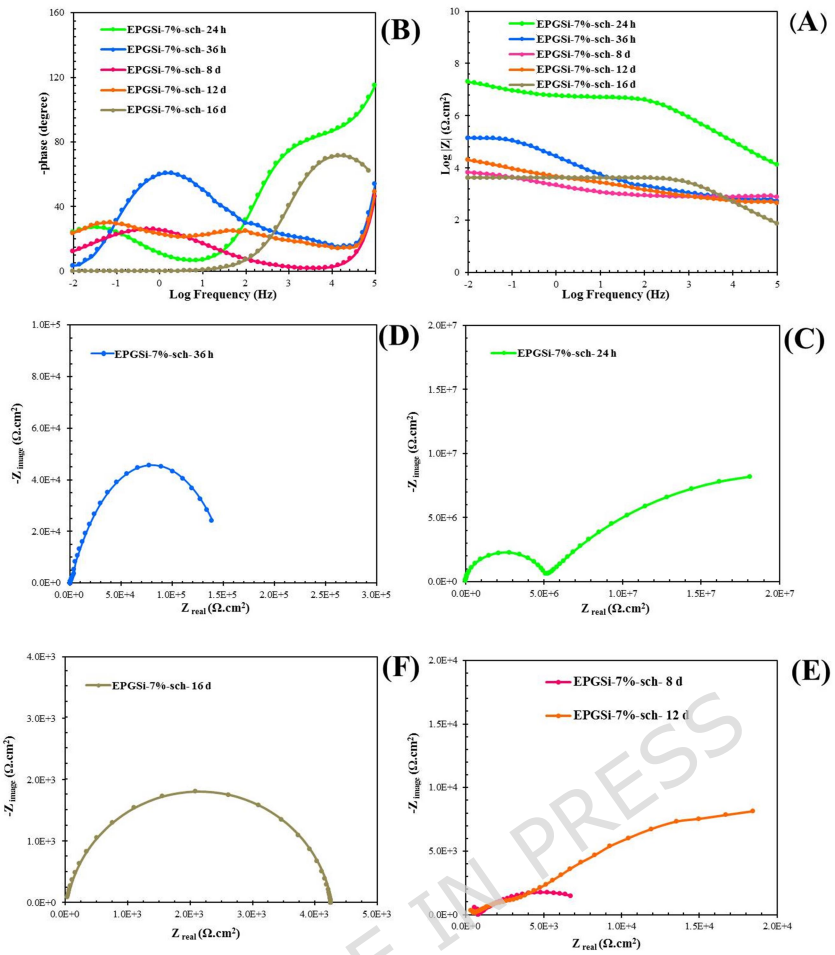

FIG. 11: EIS curves of epoxy-silane graphene oxide coating system containing electrospun core-shell fibers with 7 wt. % PVA solution scratched (A) Bode curves from 24 hr to 16 days, (B) Bode-Phase from 24 hr to 16 days, (C) Nyquist curve for 24 hours, (D) Nyquist curve for 36 hours, (E) Nyquist curves for 8 and 12 days, (F) Nyquist curve for 16 days immersion in 3.5 wt. % sodium chloride solution.

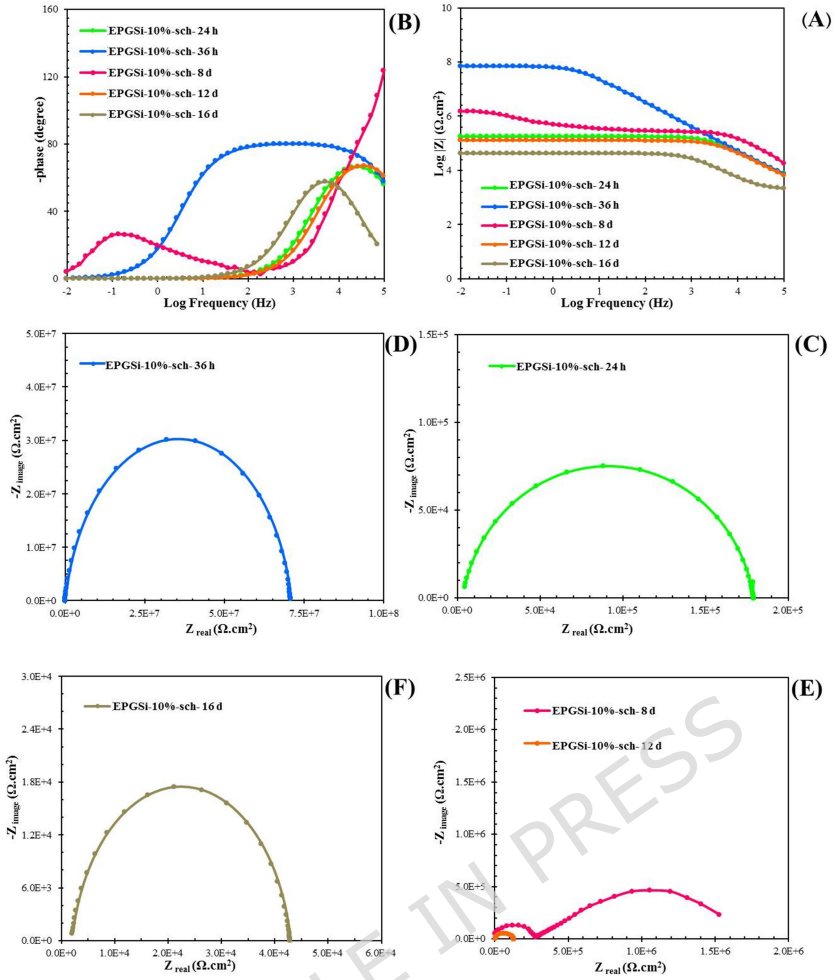

FIG. 12: EIS curves of epoxy-silane graphene oxide coating system containing electrospun core-shell fibers with 10 wt. % PVA solution scratched (A) Bode curves from 24 hr to 16 days, (B) Bode-Phase from 24 hr to 16 days, (C) Nyquist curve for 24 hours, (D) Nyquist curve for 36 hours, (E) Nyquist curves for 8 and 12 days, (F) Nyquist curve for 16 days immersion in 3.5 wt. % sodium chloride solution.

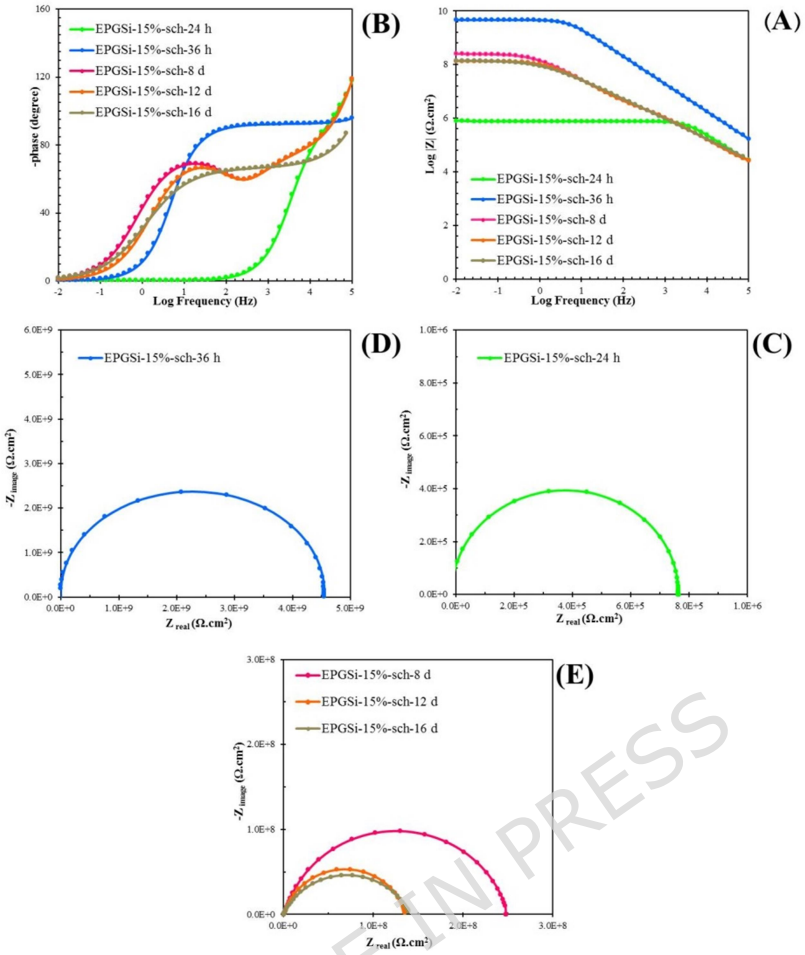

FIG. 13: EIS curves of epoxy-silane graphene oxide coating system containing electrospun core-shell fibers with 15 wt. % PVA solution scratched (A) Bode curves from 24 hr to 16 days, (B) Bode-Phase from 24 hr to 16 days, (C) Nyquist curve for 24 hours, (D) Nyquist curve for 36 hours, (E) Nyquist curves for 8, 12 and 16 days immersion in 3.5 wt. % sodium chloride solution.

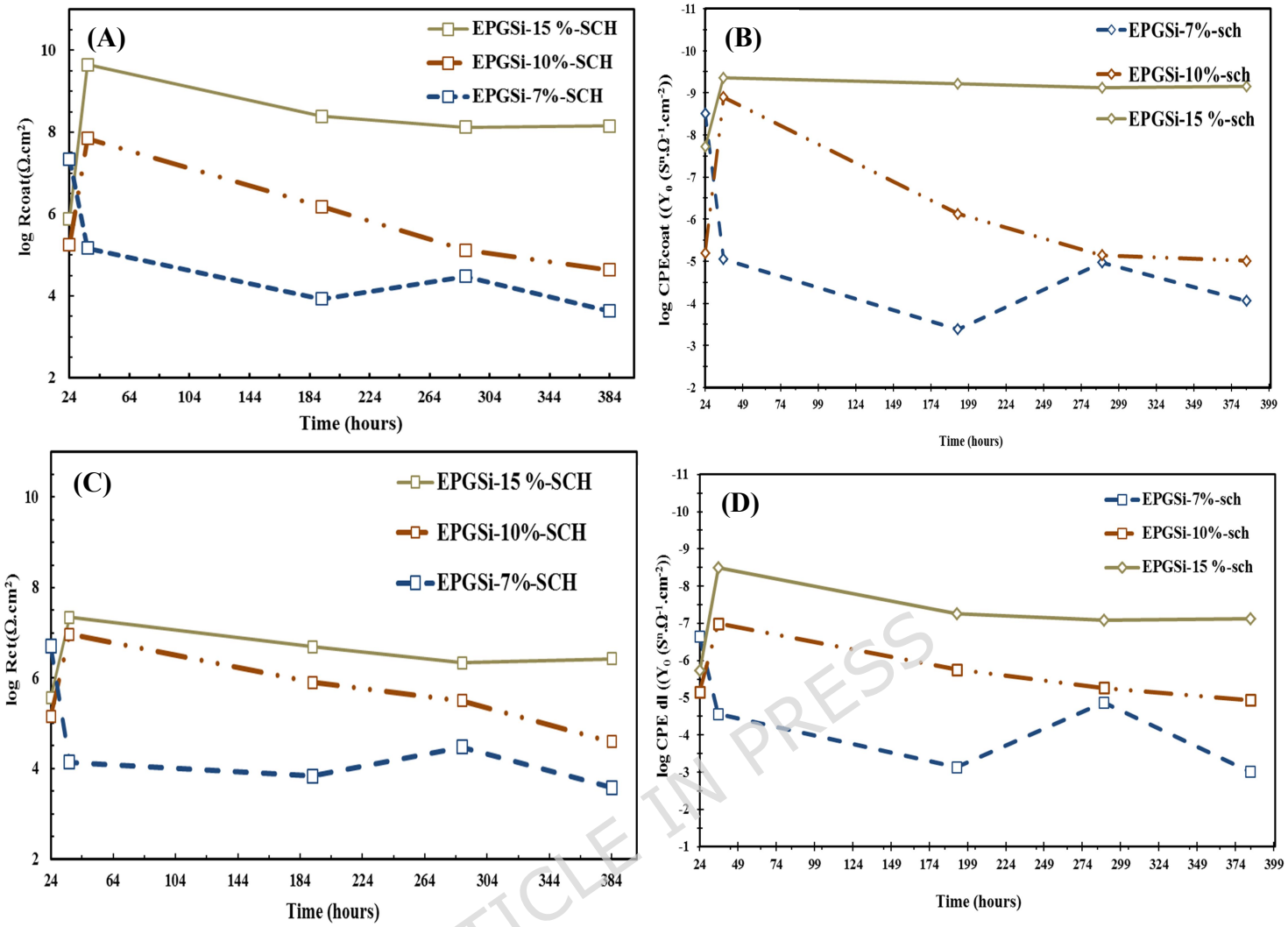

FIG. 14: The changes of (A) Equivalent capacitance of coating system, (B) Resistance of coating system, (C) Capacitance of double layer and (D) Charge transfer resistance of epoxy-silane graphene oxide coating system containing core-shell fibers electrospun with PVA solution 7, 10 and 15 wt. % contains scratches after 16 days of immersion in 3.5 wt. % solution of sodium chloride.

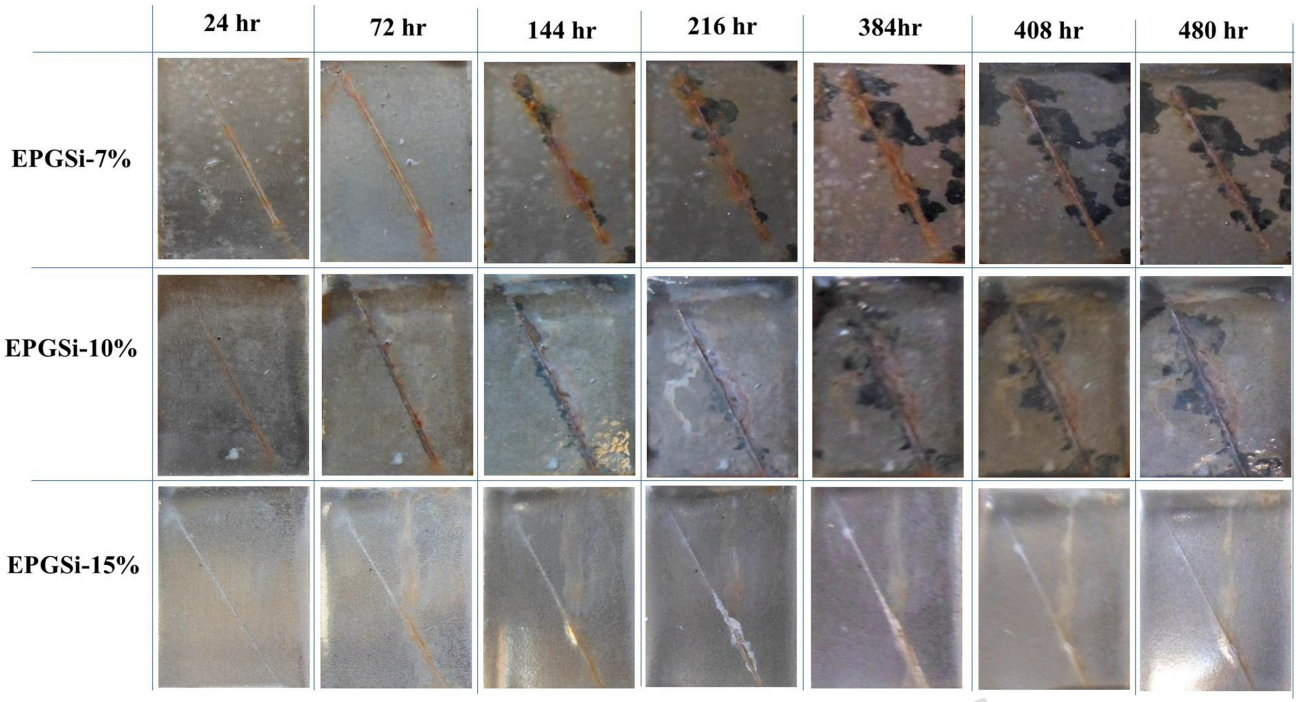

FIG. 15: Digital images of salt spray test from the surface area of the coating samples containing core-shell fibers electrospun in concentrations of 7, 10 and 15 wt. % PVA shell and after 480 hours exposed to 5±1 wt. % sodium chloride environment.

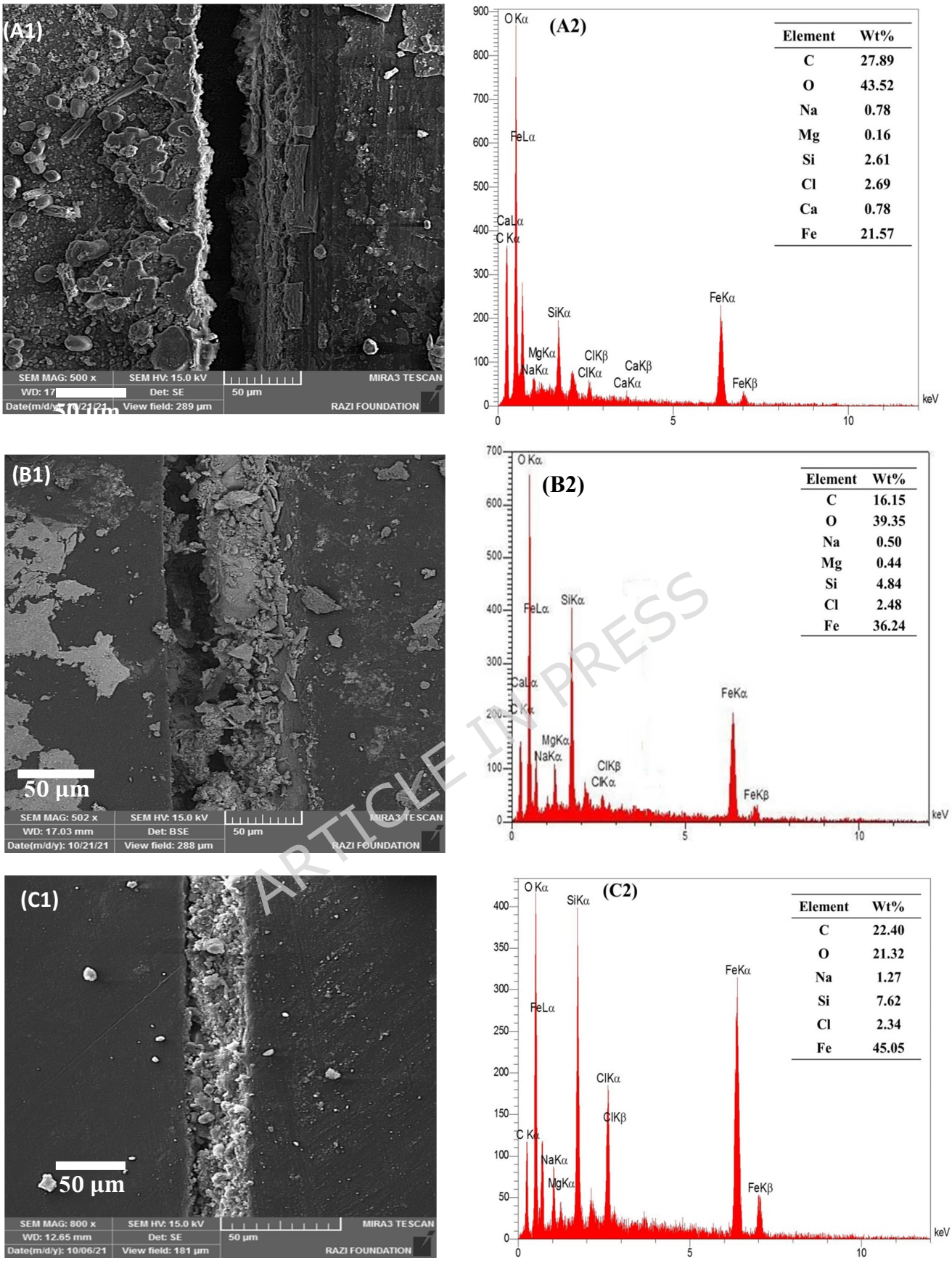

FIG. 16: The FE-SEM images and EDS analysis from the surface morphology of the scratched area of coatings containing electrospun core-shell fibers in concentrations of 7 (A1 and A2), 10 (B1 and B2) and 15 wt. % (C1 and C2) after 480 hours exposed to the environment 5±1 wt. % sodium chloride.

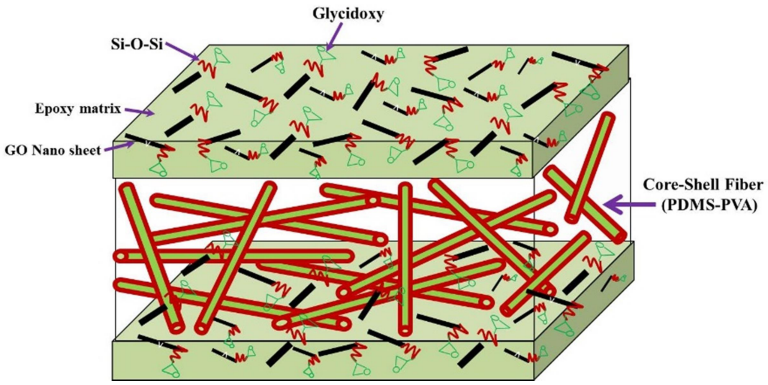

FIG. 17: The schematic picture of the structure of epoxy-silane graphene oxide nanocomposite coating system containing core-shell fibers.

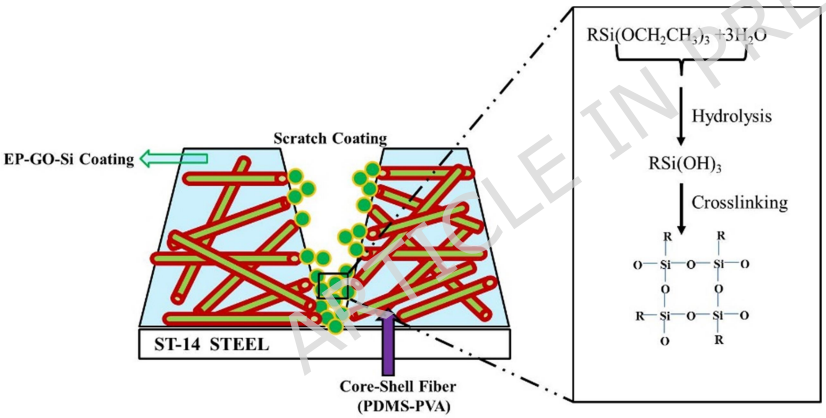

FIG. 18: The schematic picture of the self-healing mechanism of the silane-oxide-graphene epoxy nanocomposite coating system containing core-shell fibers after creating.

Table 1: Electrochemical parameters related to fitting the impedance curves of the epoxy-silanized graphene oxide coating system containing electrospun core-shell fibers with 7 wt. % PVA solution with EEC during 148 days of immersion in 3.5 wt. % chloride solution sodium.

Sample	Time (d)	R_s ($\Omega.cm^2$)	CPE_c ($Y_0(S^n.\Omega^{-1}.cm^{-2})$)	n	R_c ($\Omega.cm^2$)	CPE_{dl} ($Y_0(S^n.\Omega^{-1}.cm^{-2})$)	n	R_{ct} ($\Omega.cm^2$)
EPGSi-7%	1	6.521×10^{3}	1.59×10^{-10}	0.981	5.95×10^{9}	-	-	-
	5	1.138×10^{4}	2.036×10^{-10}	0.972	1.01×10^{9}	-	-	-
	12	1.466×10^{4}	4.63×10^{-10}	0.965	9.09×10^{8}	-	-	-
	18	7.261×10^{3}	6.19×10^{-10}	0.961	5.2×10^{8}	-	-	-
	29	3.867×10^{4}	1.012×10^{-9}	0.947	2.61×10^{8}	-	-	-
	46	3.427×10^{4}	3.71×10^{-10}	0.935	8.06×10^{8}	-	-	-
	63	2.567×10^{4}	1.825×10^{-7}	0.835	4.81×10^{6}	5.926×10^{-6}	0.731	7.18×10^{5}
	78	8.067×10^{4}	5.184×10^{-8}	0.851	5.78×10^{6}	2.371×10^{-6}	0.769	9.02×10^{5}
	99	8.496×10^{4}	6.238×10^{-7}	0.814	3.11×10^{6}	8.174×10^{-6}	0.710	4.93×10^{5}
	120	1.471×10^{4}	8.963×10^{-7}	0.782	3.01×10^{6}	8.869×10^{-6}	0.693	4.71×10^{5}
	132	1.297×10^{4}	1.954×10^{-7}	0.827	4.63×10^{6}	5.195×10^{-6}	0.949	7.68×10^{5}
	148	7.601×10^{3}	7.384×10^{-7}	0.741	1.52×10^{5}	3.917×10^{-5}	0.674	2.59×10^{4}

Table 2: Electrochemical parameters related to fitting the impedance curves of the epoxy-silanized graphene oxide coating system containing electrospun core-shell fibers with 10 wt. % PVA solution with EEC during 148 days of immersion in 3.5 wt. % chloride solution sodium.

Sample	Time (d)	R_s ($\Omega.cm^2$)	CPE_c (Y_0 ($S^n.\Omega^{-1}.cm^{-2}$))	n	R_c ($\Omega.cm^2$)	CPE_{dl} (Y_0 ($S^n.\Omega^{-1}.cm^{-2}$))	n	R_{ct} ($\Omega.cm^2$)
EPGSi-10%	1	100	1.01×10^{-10}	0.99	8.26×10^{10}	-	-	-
	5	1.748×10^{4}	1.97×10^{-10}	0.98	7.81×10^{10}	-	-	-
	12	1.256×10^{3}	2.94×10^{-10}	0.98	2.51×10^{10}	-	-	-
	18	6.472×10^{3}	8.94×10^{-10}	0.97	8.01×10^{9}	-	-	-
	29	3.670×10^{4}	3.84×10^{-9}	0.96	2.96×10^{8}	-	-	-
	46	5.670×10^{3}	1.35×10^{-9}	0.97	4.91×10^{8}	-	-	-
	63	5.670×10^{3}	4.13×10^{-9}	0.96	1.74×10^{8}	-	-	-
	78	5.670×10^{3}	2.13×10^{-9}	0.96	2.65×10^{8}	-	-	-
	99	4.670×10^{3}	6.93×10^{-8}	891.0	2.69×10^{7}	1.37×10^{-6}	0.784	2.95×10^{5}
	120	1.148×10^{4}	8.941×10^{-7}	865.0	2.04×10^{7}	1.28×10^{-6}	0.712	1.635×10^{5}
	132	1.880×10^{4}	3.381×10^{-8}	897.0	2.93×10^{7}	1.02×10^{-6}	0.795	5.19×10^{5}
	148	1.328×10^{4}	7.357×10^{-7}	851.0	1.17×10^{7}	1.52×10^{-6}	0.715	2.16×10^{5}

Table 3: Electrochemical parameters related to fitting the impedance curves of the epoxy-silanized graphene oxide coating system containing electrospun core-shell fibers with 15 wt. % PVA solution with EEC during 148 days of immersion in 3.5 wt. % chloride solution sodium.

Sample	Time (d)	R_s ($\Omega.cm^2$)	CPE_c (Y_0 ($S^n.\Omega^{-1}.cm^{-2}$))	n	R_c ($\Omega.cm^2$)	CPE_{dl} (Y_0 ($S^n.\Omega^{-1}.cm^{-2}$))	n	R_{ct} ($\Omega.cm^2$)
EPGSi-15 %	1	7.91×10^{3}	1.08×10^{-10}	0.995	8.5×10^{10}	-	-	-
	5	1.32×10^{3}	2.4×10^{-10}	0.981	5.1×10^{10}	-	-	-
	12	6.48×10^{3}	4.7×10^{-10}	0.973	1.01×10^{10}	-	-	-
	18	3.34×10^{3}	6.2×10^{-10}	0.971	8.3×10^{9}	-	-	-
	29	2.28×10^{2}	6.5×10^{-10}	0.971	8.1×10^{9}	-	-	-
	46	1.054×10^{4}	5.7×10^{-11}	0.997	1.17×10^{11}	-	-	-
	63	2.669×10^{3}	4.13×10^{-10}	0.984	1.4×10^{10}	-	-	-
	78	1.322×10^{3}	1.05×10^{-10}	0.986	9.03×10^{10}	-	-	-
	99	1.012×10^{3}	5.71×10^{-10}	0.987	8.41×10^{9}	-	-	-
	120	1.351×10^{4}	3.48×10^{-9}	0.953	1.11×10^{8}	2.67×10^{-9}	0.892	1.3×10^{7}
	132	1.681×10^{4}	9.18×10^{-9}	0.961	2.03×10^{8}	5.36×10^{-9}	0.897	3.4×10^{6}
	148	1.886×10^{3}	4.75×10^{-8}	0.901	4.21×10^{7}	2.36×10^{-7}	0.851	9.83×10^{5}

Table 4: Electrochemical parameters related to fitting the impedance curves of epoxy-silane graphene oxide coating system containing electrospun core-shell fibers with 7 wt. % scratched PVA solution with EEC during 16 days of immersion in 3.5 wt. % sodium chloride solution.

Sample	Time (d)	R_s ($\Omega.cm^2$)	CPE_c (Y_0 ($S^n.\Omega^{-1}.cm^{-2}$))	n	R_c ($\Omega.cm^2$)	CPE_{dl} (Y_0 ($S^n.\Omega^{-1}.cm^{-2}$))	n	R_{ct} ($\Omega.cm^2$)
EPGSi-7%-sch	24 h	6972	3.055×10^{-9}	0.92	2.197×10^{7}	2.291×10^{-7}	0.61	5.017×10^{6}
	36 h	4.704	8.909×10^{-6}	0.78	1.453×10^{5}	2.752×10^{-5}	0.57	1.371×10^{4}
	8 d	753	4.164×10^{-4}	0.53	8.379×10^{3}	7.398×10^{-4}	0.50	6.875×10^{3}
	12 d	623	1.072×10^{-5}	0.62	3.021×10^{4}	1.353×10^{-5}	0.58	2.953×10^{4}
	16 d	415	8.74×10^{-4}	0.49	4.266×10^{3}	9.962×10^{-4}	0.48	3.816×10^{3}

Table 5: Electrochemical parameters related to fitting the impedance curves of epoxy-silane graphene oxide coating system containing electrospun core-shell fibers with 10 wt. % scratched PVA solution with EEC during 16 days of immersion in 3.5 wt. % sodium chloride solution.

Sample	Time (d)	R_s ($\Omega.cm^2$)	CPE_c (Y_0 ($S^n.\Omega^{-1}.cm^{-2}$))	n	R_c ($\Omega.cm^2$)	CPE_{dl} (Y_0 ($S^n.\Omega^{-1}.cm^{-2}$))	n	R_{ct} ($\Omega.cm^2$)
EPGSi-10%-sch	24 h	11276	6.384×10^{-6}	0.84	1.763×10^{5}	7.012×10^{-6}	0.83	1.438×10^{5}
	36 h	11327	1.257×10^{-9}	0.85	7.019×10^{7}	1.021×10^{-7}	0.67	9.271×10^{6}
	8 d	29710	7.427×10^{-7}	0.72	1.531×10^{6}	1.743×10^{-6}	0.89	7.931×10^{5}
	12 d	11276	7.169×10^{-6}	0.69	1.296×10^{5}	2.482×10^{-6}	0.86	3.158×10^{5}
	16 d	7962	9.751×10^{-6}	0.63	4.261×10^{4}	1.159×10^{-5}	0.62	3.957×10^{4}

Table 6: Electrochemical parameters related to fitting the impedance curves of epoxy-silane graphene oxide coating system containing electrospun core-shell fibers with 15 wt. % scratched PVA solution with EEC during 16 days of immersion in 3.5 wt. % sodium chloride solution.

Sample	Time (d)	R_s ($\Omega.cm^2$)	CPE_c (Y_0 ($S^n.\Omega^{-1}.cm^{-2}$))	n	R_c ($\Omega.cm^2$)	CPE_{dl} (Y_0 ($S^n.\Omega^{-1}.cm^{-2}$))	n	R_{ct} ($\Omega.cm^2$)
EPGSi-15%-sch	24 h	13169	1.857×10^{-8}	0.82	7.760×10^{5}	1.864×10^{-6}	0.75	3.728×10^{5}
	36 h	9612	4.41×10^{-10}	0.96	4.448×10^{9}	3.27×10^{-9}	0.89	2.175×10^{7}
	8 d	19031	6.158×10^{-10}	0.93	2.451×10^{8}	5.628×10^{-8}	0.83	4.909×10^{6}
	12 d	19031	7.628×10^{-10}	0.86	1.312×10^{8}	8.156×10^{-8}	0.80	2.173×10^{6}
	16 d	17321	7.121×10^{-10}	0.87	1.41×10^{8}	7.476×10^{-8}	0.81	2.671×10^{6}